30–60 Day Atmospheric Oscillations: Composite Life Cycles of Convection and Circulation Anomalies

THOMAS R. KNUTSON

Geophysical Fluid Dynamics Laboratory/NOAA, Princeton University, Princeton, NJ 08542

KLAUS M. WEICKMANN*

Center for Climatic Research, University of Wisconsin, Madison, WI 53706

(Manuscript received 4 March 1986, in final form 31 December 1986)

ABSTRACT

Life cycles of the 30–60 day atmospheric oscillation were examined by compositing 30–60 day filtered NMC global wind analyses (250 mb and 850 mb) and outgoing longwave radiation (OLR) for the years 1979–84. Separate composite life cycles were constructed for the May–October and November–April seasons using empirical orthogonal function analysis of the large-scale divergent wind field (250 mb velocity potential) to define the oscillation's phase. Monte Carlo simulations were used to assess the statistical significance of the composite OLR and vector wind fields.

Large-scale (wavenumber one) tropical divergent wind features propagate eastward around the globe throughout the seasonal cycle. The spatial relationships between these propagating circulation features and OLR are shown using sequences of composite maps. Good agreement exists between areas of upper-air divergence and areas of convection inferred from the OLR satellite data. Convection anomalies are smaller over tropical Africa and South America than over the Indian and western Pacific oceans. Anomalies of OLR are nearly negligible over cooler tropical sea surfaces. Fluctuations in summer monsoon region convection are influenced by the global-scale eastward-moving wave.

The oscillation's vertical structure varies with latitude. In the tropics, upper-level and lower-level tropospheric wind anomalies are about 180° out of phase. Poleward of about 20°, there is no pronounced phase shift between levels. In tropical and subtropical latitudes, analysis of the nondivergent circulation composites at 250 mb (ψ_{250}) reveals cyclones to the east of the convection and anticyclones alongside or west of the convection. While convection anomalies are most pronounced in the summer hemisphere tropics, the tropical and subtropical ψ_{250} features are most prominent in the winter hemisphere. There is some evidence of symmetry of cyclonic and anticyclonic circulations about the equator.

A subset of the composite extratropical vector wind fields were statistically significant (95% level) at 850 and 250 mb in the winter hemisphere (25°–85° latitude), based upon a Monte Carlo simulation. During the November–April season, the East Asian jet is retracted toward Asia when positive 30–60 day convection anomalies are occurring over the equatorial Indian Ocean. The eastward shift of convection into the western and central Pacific is accompanied by a series of circulation features over northern Asia and an eastward extension of the East Asian jet. During the May–October season, the shift of large-scale tropical convection anomalies from the Indian Ocean and Indian monsoon regions to the tropical western Pacific is followed (10–15 days later) by the occurrence of strengthened westerlies over southern Australia. In contrast, the extratropical "response" in the summer hemisphere for both the May–October and November–April seasons was not statistically significant.

1. Introduction

Large-scale circulation and convection features in the tropical atmosphere have been observed to fluctuate with certain characteristic time scales and spatial patterns. Two such global-scale phenomena are the El Niño/Southern Oscillation, which has a time scale of about 2 to 6 years, and the tropical 30–60 day oscillation.

The 30–60 day oscillation, which is not well resolved in traditional monthly averaged statistics, was detected by Madden and Julian (1971, 1972) using spectral analysis of tropical rawinsonde data. More recently, the general characteristics of the oscillation have been studied using a variety of data sources, observations periods, and analysis methods.

Some important characteristics of the oscillation are listed below. For a more comprehensive review, see Knutson, Weickmann, and Kutzbach (1986, hereafter referred to as KWK).

- The oscillation is characterized by global-scale tropical wind and convection anomalies, including a

* Present affiliation: U.S. Department of Commerce, NOAA/ERL, 325 Broadway, Boulder, CO 80303.

modulation of the Northern Hemisphere and Southern Hemisphere summer monsoon activity.

- The oscillation is not strictly periodic, but has a preferred time scale of about 30 to 60 days.
- Convection and circulation anomalies associated with the oscillation tend to propagate eastward with time.
- In the tropics, 30–60 day zonal wind anomalies in the lower troposphere are out of phase with those in the upper troposphere (Madden and Julian, 1971; 1972).
- The phenomenon occurs throughout the seasonal cycle with no systematic seasonal variation in amplitude or periodicity (Anderson et al., 1984). However, in the present study we will show that the oscillation does exhibit seasonality in the locations of maximum OLR variability and in the extratropical "response".
- Some evidence exists for an association between tropical convection fluctuations and midlatitude circulation anomalies on 30–60 day time scales (Weickmann et al., 1985, hereafter referred to as WLK; Lau and Phillips, 1986).
- Oscillations of a similar time scale have been observed in the tropical oceans. For example, Mysak and Mertz (1984) reported on 40–60 day oscillations of longshore currents and ocean temperatures in the western Indian Ocean.
- Intraseasonal (25–40 day) atmospheric oscillations, characterized by eastward propagation of large-scale tropical wind anomalies, have been found in general circulation models (GCM's) by Lau and Lau (1986) and Hayashi and Sumi (1986). Goswami and Shukla (1984) have found 20–40 day oscillations in a zonally symmetric GCM.

The eastward propagation of 30–60 day outgoing longwave radiation (OLR) anomalies has been noted by Weickmann (1983), WLK, KWK, Lau and Chan (1985, 1986), Murakami et al. (1986) and others. The characteristic propagation speed for this phenomenon is 3–6 m s^{-1}, and the propagation occurs over the tropical Indian and western Pacific oceans.

Eastward-propagating large-scale circulation features on 30–60 day time scales have been noted by Lorenc (1984) and Krishnamurti et al. (1985), who studied velocity potential for the FGGE year. Madden and Julian (1972), Parker (1973), KWK, and others have noted similar propagation characteristics for tropical zonal wind anomalies. In contrast to the OLR anomalies, the circulation features noted in these studies have been observed to propagate around the entire globe during an oscillation and have typical propagation speeds of 10 m s^{-1}.

The propagation characteristics of OLR and tropical circulation features can be summarized using Hovmöller diagrams of 30–60 day filtered data. For example, Fig. 1 shows 30–60 day anomalies for 1981 of NMC velocity potential data at 250 mb (χ_{250}) and 850 mb (χ_{850}), zonal winds (U250, U850), 850 mb divergence (δ_{850}) and OLR in time–longitude format. The details of the data sets and time filter will be presented in section 2. A reference line representing a wavenumber-1 eastward-propagating signal with a 45-day period ($\sim$10 m s^{-1} propagation speed) is drawn at the same location on each diagram.

A comparison of the anomalies in Fig. 1 (averaged 5°N–5°S) indicates the following: 1) the most consistent eastward propagation occurs for the velocity potential, although it is evident for each of the variables; 2) 250 and 850 mb tropical circulation anomalies are approximately 180° out of phase; 3) the 850 mb divergence anomalies show the least evidence for systematic eastward propagation, although the largest-scale features tend to move eastward; and 4) OLR anomalies are of largest amplitude in the eastern hemisphere, and OLR anomalies in this sector often propagate eastward more slowly than 10 m s^{-1} (reference line). Time-filtered OLR data for other years are shown in Murakami et al. (1986; Figs. 4–5).

Because the eastward propagation of anomalies may be an important element in producing the oscillation's fundamental time scale, it is important to fully document the spatial and temporal relationships between the globally propagating circulation anomalies and the slower-moving OLR anomalies over the Indian and western Pacific oceans. In the present study, NMC 250 and 850 mb circulation data and OLR data for six years (1979–84) are combined into a single *composite analysis* in order to more clearly depict these relationships for a typical oscillation. The 30–60 day 250 mb velocity potential (χ_{250}) data, which show distinct global-scale eastward propagation, are used to construct a composite index for life cycles of the oscillation.

Although Anderson et al. (1984) show that there is no systematic seasonal variation in the oscillation's time scale, we find that its spatial structure exhibits seasonal changes. These changes are highlighted in the present study by constructing separate life cycles for the May–October and November–April seasons.

In addition to the tropical circulation/OLR relationships, the compositing technique is used to study the tropical/subtropical rotational (nondivergent) circulation features accompanying the eastward-propagating convection anomalies. Vector wind composites for the entire globe are used to show the extratropical circulation patterns associated with the tropical oscillation. Fluctuations in low-level winds and convection in the Indian monsoon region are demonstrated to be temporally related to the global-scale χ_{250} "wave" during May–October.

The composite life cycles provide a means of comparing the observed 30–60 day oscillation with intraseasonal oscillation in GCMs. In particular, the composite GCM study of Lau and Lau (1986) used an analysis procedure similar to ours, which facilitates comparisons between the two studies. With respect to

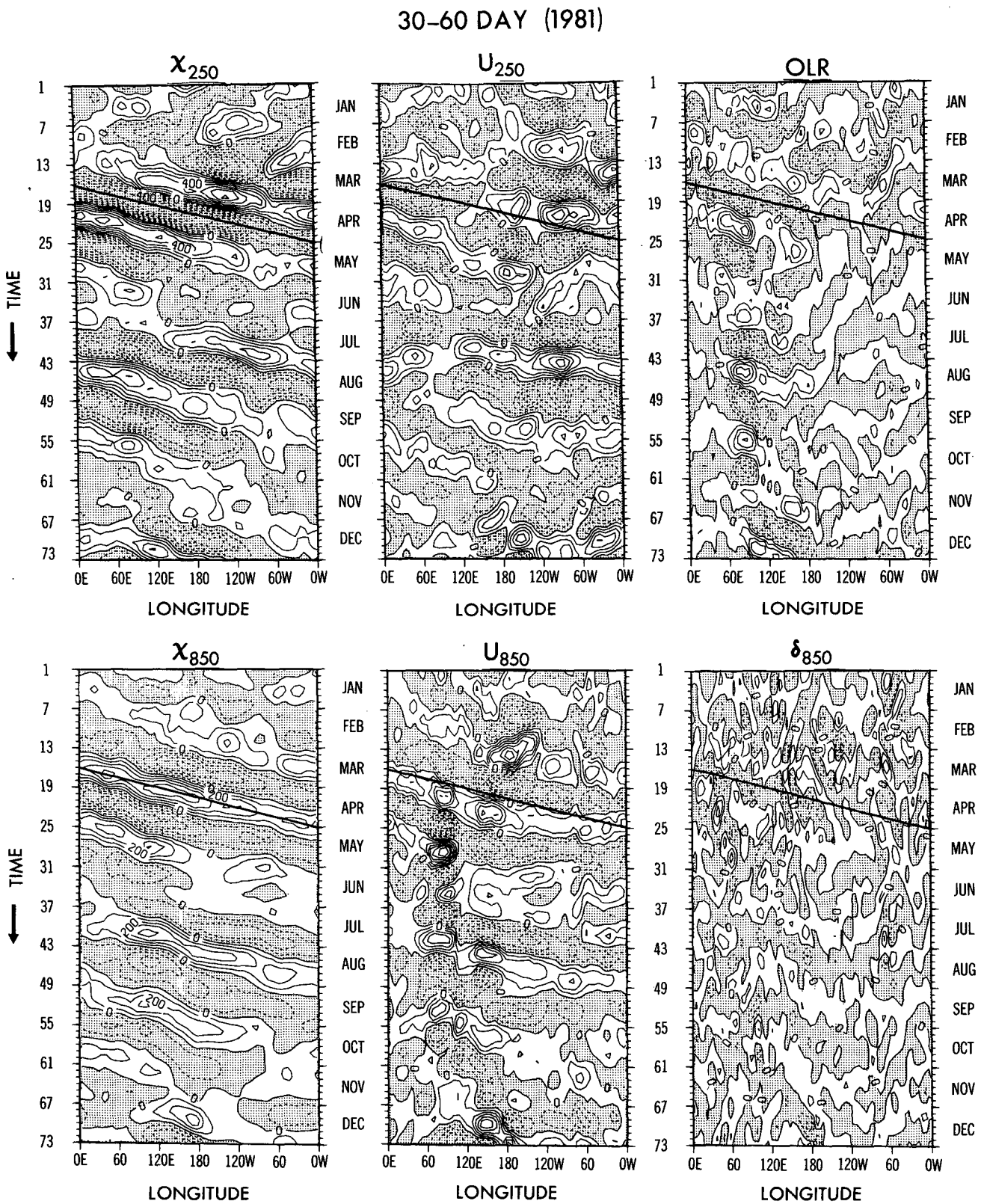

FIG. 1. Time vs longitude diagrams of 30–60 day filtered anomalies (averaged 5°N–5°S) for 1981. Variables and contour intervals are χ_{250} (10^6 m^2 s^{-1}); U250 (2.0 m s^{-1}); OLR (10 W m^{-2}); χ_{850} (10^6 m^2 s^{-1}); U850 (1.0 m s^{-1}); and 850 mb divergence (δ_{850}, 10^{-6} s^{-1}). Negative anomalies are shaded; the reference lines represent an eastward-propagating (~10 m s^{-1}) signal with a period of 45 days.

operational forecasting and real-time monitoring efforts, the life cycles provide a framework for identifying fluctuations in large-scale tropical and extratropical weather patterns which could be associated with the 30–60 day tropical oscillations.

2. Data and methods

a. *Data description and filtering*

The primary data used in this study are five-day-averaged global grids of NMC analyzed winds (250 and 850 mb) and outgoing longwave radiation (OLR) from polar-orbiting satellites. The spatial resolution is 5° latitude by 5° longitude, and the period covered by the filtered data (all variables) is 17–21 March 1979 to 2–6 November 1984. By using only data obtained after September 1978, we have excluded the nearly nondivergent NMC tropical and subtropical wind analyses obtained using the Hough analysis technique (Cooley, 1974; Rosen and Salstein, 1980). For limited periods, we have NMC wind data on 12 levels, which we use in a case study to illustrate the vertical structure of the tropical divergent wind anomalies.

The five-day averages, or pentads, were formed by averaging ten nonoverlapping twice-daily analyses. Missing data were linearly interpolated; no data gaps of greater than 10 days occurred. The means, annual and semiannual cycles, which are described more fully in Kutzbach and Weickmann (1984), were removed by subtracting the mean and first two Fourier harmonics of the average 73-pentad seasonal cycle from the data. More details on the data set and prefiltering methods may be found in WLK and KWK. The period of record used in the present study (about six years) is somewhat shorter than the dataset used in WLK and KWK as a result of excluding 1974–78.

In order to emphasize only the 30–60 day fluctuations in the data, a 31-point bandpass filter (response shown in Fig. 2) was applied to each time series of all the variables used in the study. The filtered time series were subsequently used to form the composite maps. The particular time scale selected was shown to be an appropriate one by KWK, although various other studies have emphasized slightly different period ranges (e.g., 40–50 days).

b. *Interpretation of anomalies*

As in KWK, we will focus on OLR anomalies occurring within about 20° of the equator, which we assume are correlated strongly to regions of increased (negative OLR anomalies) or decreased (positive OLR anomalies) large-scale convective activity.

From the NMC vector wind data, we derived streamfunction and velocity potential fields for both 250 and 850 mb. The streamfunction, ψ, is defined by

$$\nabla^2\psi = \zeta$$

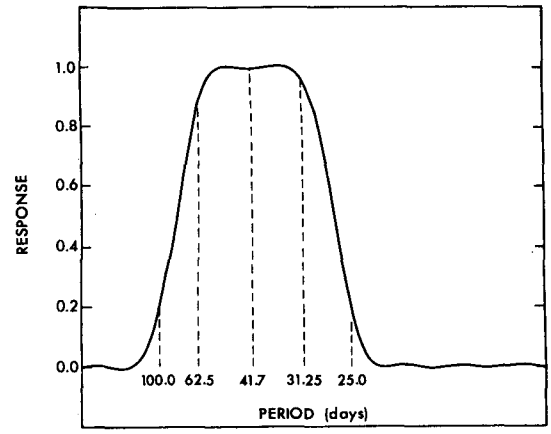

FIG. 2. Response as a function of period of the 31-point filter used in this study when applied to data sampled once per 5 days. Since our data were 5-day averaged prior to filtering, the net response differs slightly from that shown.

where ζ is the relative vorticity, defined as

$$\zeta = \frac{1}{r\cos\phi}\left[\frac{\partial v}{\partial\lambda} - \frac{\partial}{\partial\phi}(u\cos\phi)\right]$$

where ϕ is latitude and λ is longitude. Each streamfunction and velocity potential field is adjusted to have a global mean (cosine-weighted by latitude) of zero.

Streamfunction maps may be interpreted similarly to geopotential height data in the extratropics except that the rotational (nondivergent) wind is inferred, rather than the geostrophic wind. The sign convention used is that winds travel cyclonically around a local ψ *minimum* (inferred low heights) in the Northern Hemisphere and cyclonically around a local ψ *maximum* (inferred low heights) in the Southern Hemisphere. Since the streamfunction gradient/wind magnitude relationship is independent of latitude, streamfunction is more useful for monitoring wind circulations than geopotential height in the tropics. However, streamfunction anomalies cannot be used near the equator to infer anomalies of geopotential height.

The velocity potential, χ, is defined by

$$\nabla^2\chi = \delta$$

where δ is the divergence, defined as

$$\delta = \frac{1}{r\cos\phi}\left[\frac{\partial u}{\partial\lambda} + \frac{\partial}{\partial\phi}(v\cos\phi)\right].$$

The inverse Laplacian operation smooths the smaller scale divergence features, resulting in a large-scale view of the divergent wind field. As shown in Fig. 1, within the tropics the lower level and upper level velocity potential anomalies tend to be 180° out of phase. As a result, large-scale divergence (negative χ) anomalies at upper levels are usually accompanied by large-scale convergence (positive χ) anomalies at lower levels with large-scale rising motion in the intermediate levels. The

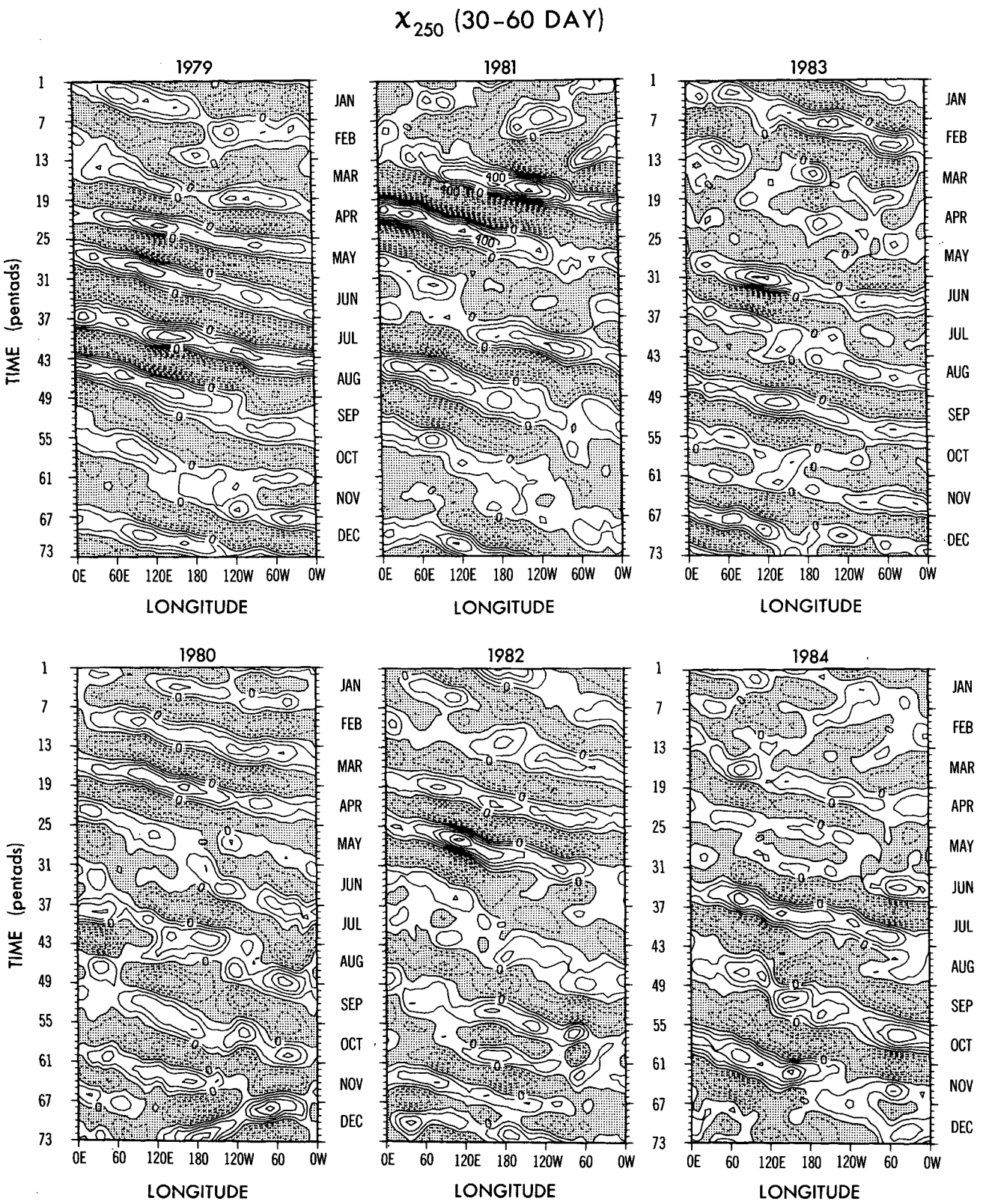

FIG. 3. Time vs longitude diagrams of 30–60 day filtered χ_{250} anomalies for the study period (1979–84). Contour interval is 1.0×10^6 m^2 s^{-1}; negative anomalies are shaded. Data were averaged from 5°N to 5°S.

divergent wind direction is toward higher values of χ, perpendicular to the contours.

In summary, we will simplify our discussion by referring to negative OLR anomalies as positive convection anomalies, by using negative χ_{250} anomalies to identify regions of anomalous rising motion, and by inferring regions of high and low height anomalies from the ψ_{250} anomalies as described above.

c. Velocity potential: Eastward propagation and vertical structure

Before presenting the results of the EOF analysis used to derive the compositing dates, we will describe the zonal propagation and vertical structure characteristics of the velocity potential data using time–longitude and longitude–pressure diagrams.

In Fig. 3, 30–60 day filtered χ_{250} data (averaged 5°N to 5°S) are displayed in time–longitude format for the years 1979–84. The most prominent features are eastward-propagating anomalies characterized by wavenumber-1 zonal structure and a propagation speed of ~ 10 m s^{-1}. Time–longitude diagrams (Fig. 1) and cross-spectral analysis (KWK) of the tropical zonal wind indicate that the global-scale wavenumber-1 structure of the circulation anomalies is not an artifact of the inverse Laplacian operation used to derive the velocity potential fields. The χ_{250} anomalies from mid-1982 to mid-1983 confirm that the 30–60 day oscillations continued to occur during the 1982–83 El Niño/Southern Oscillation event.

While Fig. 3 shows examples of westward-propagating features (e.g., from late 1980 to early 1981) or weak fluctuations, the more prominent oscillations in each year are characterized by eastward-propagating velocity potential features which can be traced for several circuits around the globe. The relatively simple spatial structure and smooth time evolution of the anomalies during major oscillation periods (such as 1979) is suggestive of the important potential role that the 30–60 day oscillation has for extended-range forcasting of large-scale divergent circulations in the tropics.

The vertical structure of divergent zonal wind anomalies during an intraseasonal oscillation is illustrated by using longitude–pressure profiles of horizontal velocity potential (χ) anomalies on 12 pressure levels. The χ fields were derived from the horizontal divergence fields of the NMC winds on each pressure level. Our analysis is limited to a case study for a 60-day period beginning 1200 UTC 1 December 1978, because our 12-level dataset covers only a fraction of the period used for the composite analysis.

In Fig. 4, longitude vs pressure profiles of the 60-day mean velocity potential (a) and horizontal divergence (b) fields are shown along with 10-day averaged anomalies (from the 60-day mean) of velocity potential (c)–(h). The data have been averaged meridionally over the Southern Hemisphere summer tropics (1°N–19°S). No time-filtering (e.g., seasonal cycle, 30–60 day) other than the 10-day averaging was applied to the data. The 12 pressure levels used are labeled on the vertical axis.

The mean χ profile (Fig. 4a) indicates a region of large-scale upper air divergent flow centered at about the dateline and extending from 400 to about 100 mb. Minimum χ values occur at 150 mb. Beneath this region of outflow is a region of lower-level convergent flow extending from 1000 to 700 mb. While evidence for these large-scale features is also present in the divergence profile (Fig. 4b), many small-scale features are present as well. A comparison of Figs. 4a and 4b indicates the degree to which the large-scale features in the divergence fields are emphasized by the inverse Laplacian operation used to form the velocity potential fields (see also 850 mb data in Fig. 1). The mean patterns for other December–January periods in our 12-level data set are similar to Fig. 4a with the exception of the anomalous December 1983–January 1983 period.

The remaining six panels (Fig. 4c–h) show the time evolution, at 10-day intervals, of χ anomalies from the 60-day mean. Based upon these panels, the following features are noted:

1) A distinct ~ 50 day oscillation occurs during the period characterized by eastward-propagating large-scale χ anomalies.

2) In the vertical direction, the anomalies have a coherent structure from 100 mb to 1000 mb, with the largest anomalies from 100 to 250 mb, smaller anomalies of opposite sign from 500 to 1000 mb, and a minimum variability in the region of phase reversal (300–500 mb).

3) Although the anomalies have vertical tilt in some of the panels, the direction of tilt varies, and prominent vertical propagation of anomalies (such as was found for the zonal wind during NH summer 1979 by Murakami and Nakazawa, 1985) is not evident. Note that an absence of vertical tilt in the velocity potential fields does not necessarily mean that other fields, such as zonal wind and streamfunction, have no vertical tilt. In any case, a more extensive composite analysis of a large data sample may be required to detect systematic tilt or vertical propagation of circulation anomalies.

Similar case studies for 60-day periods beginning December 1979, 1980, 1981 and 1982 show the same general features noted here, although as KWK and others have shown, the oscillation's amplitude, propagation and spatial structure varies from case to case. The distinct zonal and vertical structure and systematic eastward propagation noted in the above case studies suggest that the large-scale divergent flow associated with the oscillation can be successfully monitored using 5-day or 10-day averaged χ anomaly data (see Climate Analysis Center, 1985). The 150 or 200 mb levels are probably the most appropriate levels for monitoring the tropical χ anomalies.

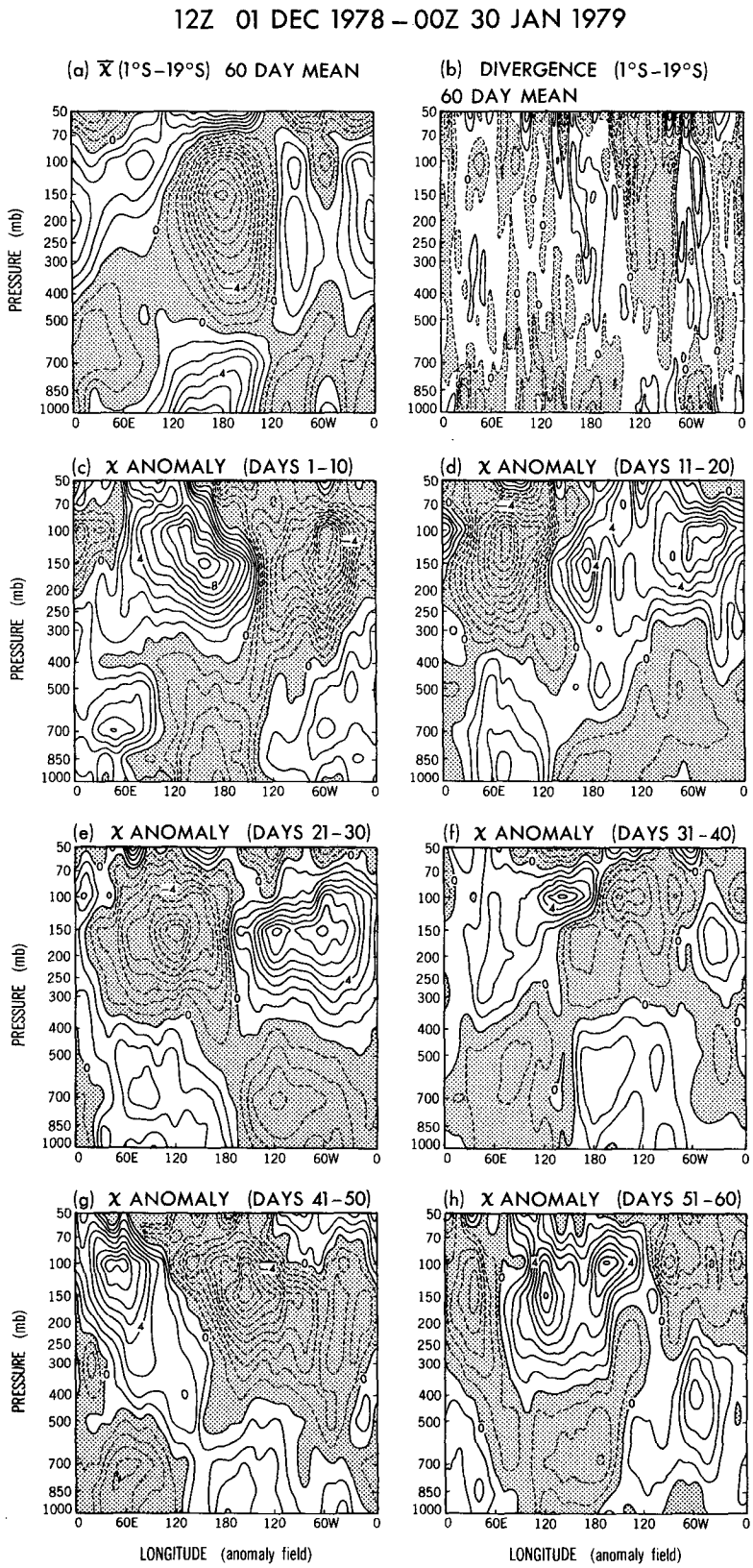

FIG. 4. Pressure vs longitude profiles of (a) 60-day mean horizontal velocity potential (χ); (b) 60-day mean horizontal velocity divergence (δ); (c–h) 10-day averaged χ anomalies at 10-day intervals. Data are averaged 1°S to 19°S for the period 1200 UTC 01 Dec 1978–0000 UTC 30 Jan 1979. Contour intervals are 1.0×10^6 m^2 s^{-1} for χ and 10^{-6} s^{-1} for δ; negative anomalies are shaded.

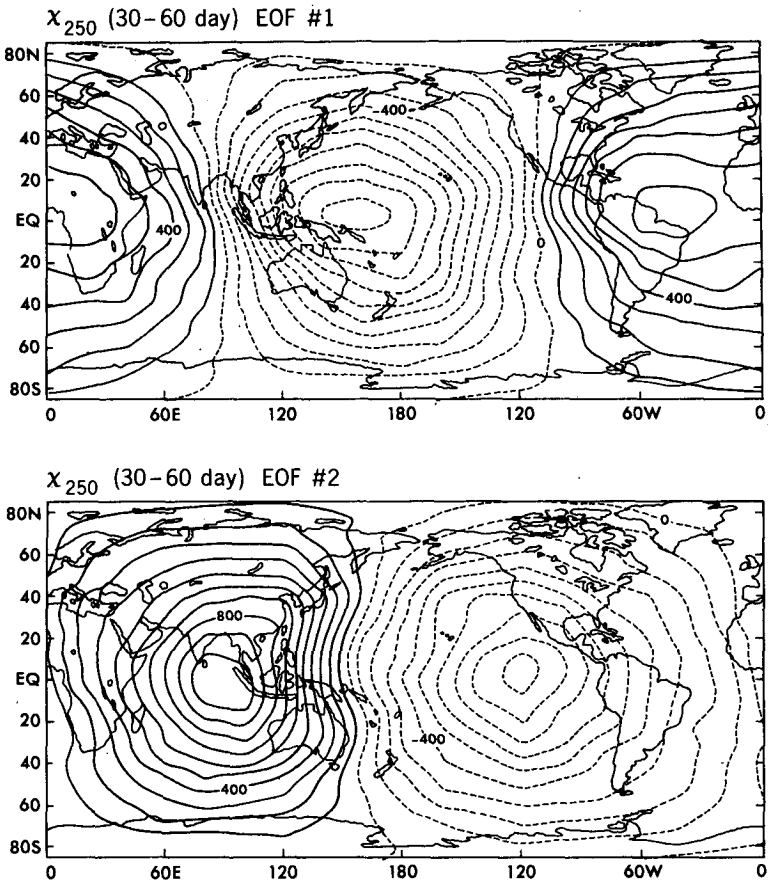

FIG. 5. First and second eigenvectors of the 30–60 day filtered χ_{250}. Contour interval is 0.01; contour labels are multiplied by 10^4.

d. Compositing procedure

Based on the relatively systematic time evolution of the 30–60 day χ_{250} anomalies, we elected to use an EOF analysis of these data to objectively determine the time variation or phase of the oscillation. The first two principal components, which describe 39% and 33% of the χ_{250} 30–60 day variance,[1] were used to select dates for compositing, as outlined below. The procedure used to derive the eigenvectors (spatial patterns) and principal components (time series) has been described in Weickmann (1983). The data were not normalized, and a single analysis was done for the full-year data, after which the composite dates were grouped into Northern Hemisphere summer and Northern Hemisphere winter seasons. The first two eigenvectors (Fig. 5) describe the propagating wavenumber-1 pattern found by Lorenc (1984) and also noted in our discussion of Fig. 3.

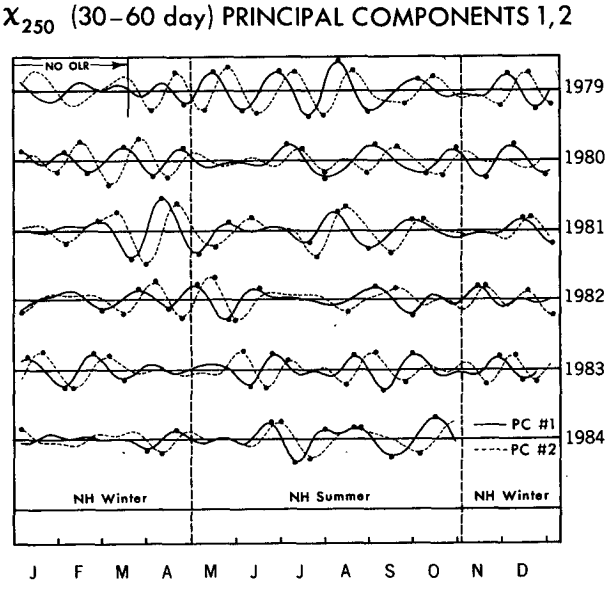

FIG. 6. First (solid) and second (dashed) principal components of the 30–60 day filtered χ_{250} with the large dots indicating significant peaks used to identify data to composite (see text for details).

[1] The 30–60 day χ_{250} fields describe 24% of the total variance of the 5-day averaged data. In comparison, the annual and semiannual cycles describe 25% of the total variance.

The first two principal components from the analysis are shown in Fig. 6. These two time series exhibit a fairly consistent phase relationship, with the first principal component (solid) leading the second (dashed) by about ¼ cycle (~10 days). The times of occurrence of maxima and minima generally differ from year to year, suggesting that the phase of the oscillation is not phase-locked to the seasonal cycle. We confirmed that the neither of the first two principal components is phase-locked to the seasonal cycle by performing *t*-tests on ensemble-averaged principal components values. The ensemble averages were obtained by averaging individual component values for the six years (1979–84) to form two seasonally averaged 73-pentad time series. None of the 146 ensemble-averaged values (73 per principal component) were significantly different from zero at the 99% level.

Four categories of dates (categories 2, 5, 8 and 11) for the composites were formed by selecting dates where time series maxima or minima exceeded a magnitude criterion as shown schematically in Fig. 7. The criterion used for selection was 0.8σ, where σ is the standard deviation of the principal component. The dates selected are indicated in Fig. 6 by large dots.

In addition to the four primary categories formed from the maxima and minima of the two time series, eight additional categories (1, 3, 4, 6, 7, 9, 10, 12) were formed by lagging the dates in the original four categories by −1 and +1 pentads (see Fig. 7). These additional categories effectively increase the temporal resolution of the composite life cycle by providing information on the time evolution of tropical convection anomalies and remote circulation responses at intermediate times during the life cycle. The number of dates included in each category is shown in Table 1 (see section 5).

While the time difference between each primary category (e.g., 2) and its associated pair of lagged categories (e.g., 1 and 3) is exactly five days, the effective time difference between adjacent categories associated with different principal components (e.g., categories 3 and 4) is not specified by the analysis. To simplify interpretation, the effective time differences between each category were estimated from the dates included in the categories and are shown on the composite map sequences in the following sections.

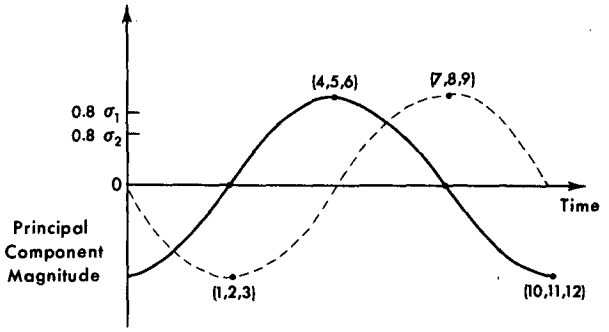

FIG. 7. Schematic illustration of the procedure used to derive the 12 categories of dates from the first two principal components of χ_{250}, represented by the solid and dashed curves.

Since the χ_{250} EOFs were used as a basis for compositing, the composite χ_{250} maps essentially reproduce the χ_{250} eigenvector patterns. Composite maps for all other variables in this study were formed by averaging 30–60 day filtered data for the sets of dates from the χ_{250} analysis. Therefore, the composite maps for other variables (e.g., OLR) should be interpreted as the typical 30–60 day anomalies accompanying the implied large-scale vertical motion (χ_{250}) anomalies.

3. Tropical convection and divergent circulation

a. Northern Hemisphere summer season

Figure 8 depicts the composite evolution (categories 1–12) of tropical convection and implied large-scale vertical motion during a "typical" oscillation for the months May–October. The darkest shading denotes *negative* OLR anomalies of more than 5 W m^{-2} (anomalous positive convective activity). The darkest solid contours (unshaded) outline regions with *positive* OLR anomalies of more than 5 W m^{-2}. Composite anomalies of more than 15 W m^{-2} were commonly found in the regions of highest OLR variability identified in KWK and WLK. Those regions are primarily in the equatorial Indian Ocean and western tropical Pacific.

The larger-scale features denoted by the lighter contours and lighter shading are the composite χ_{250} anomalies. Negative anomalies (large-scale rising motion) are denoted by the light shading. While these composites were constructed using EOF analysis of the χ_{250} as a basis for selecting dates, similar χ_{250} and OLR patterns were obtained from an 11-year dataset (1974–84) using the first two principal components of 30–60 day filtered OLR as the indices for selecting dates to composite. The composite χ_{250} patterns obtained using the 11-year dataset were weaker than those in Fig. 8, partly because of the inclusion of nearly nondivergent tropical wind fields for the years 1974–78.

A reasonable correspondence between the implied vertical motion and convection anomalies exists in all the categories. As expected, based on Hovmöller diagrams in Fig. 3, the χ_{250} pattern moves fairly smoothly to the east throughout the life cycle. As the composite dates are lagged by −1, 0, and +1 pentads (e.g., categories 1, 2 and 3) the OLR and χ_{250} features move eastward without much decrease in amplitude, confirming the strong preference for eastward propagation of large-scale tropical divergence patterns on the 30–60 day time scale. Positive convection anomalies occur in various regions throughout the tropics as the rising motion propagates around the globe, and anomalies are smaller in spatial extent over the eastern Pacific and Central America and practically negligible over the convectively active regions of the tropical Atlantic

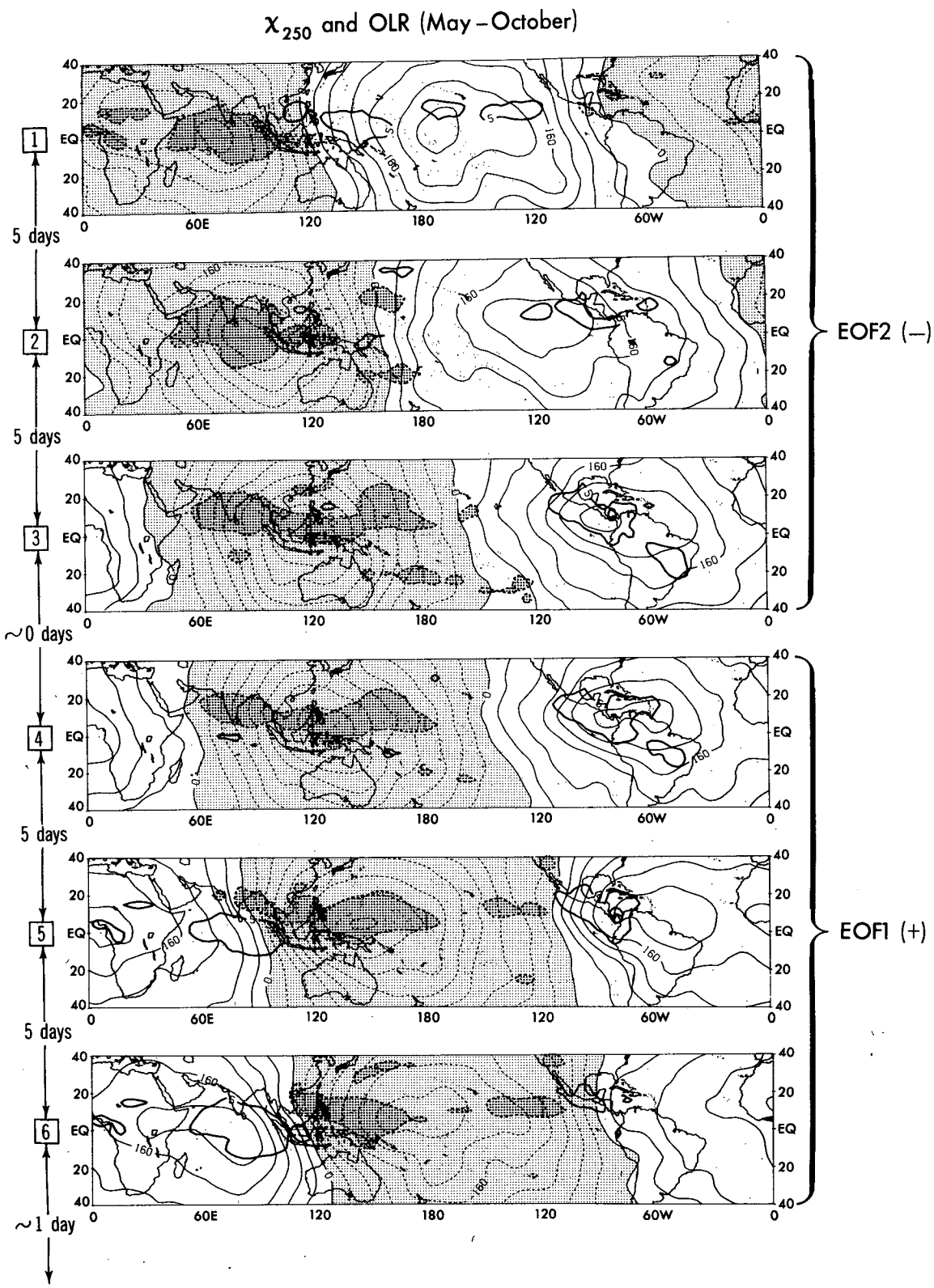

FIG. 8. Northern Hemisphere summer composite χ_{250} anomalies (light contours and shading) with composite OLR anomalies of 5 W m^{-2} or more superimposed (dark contours with dark shading for negative regions). Contour interval of χ_{250} is 4.0×10^5 m^2 s^{-1}; negative values are shaded. Boxed numbers indicate the category number; the parent EOF and estimated time between categories is also shown.

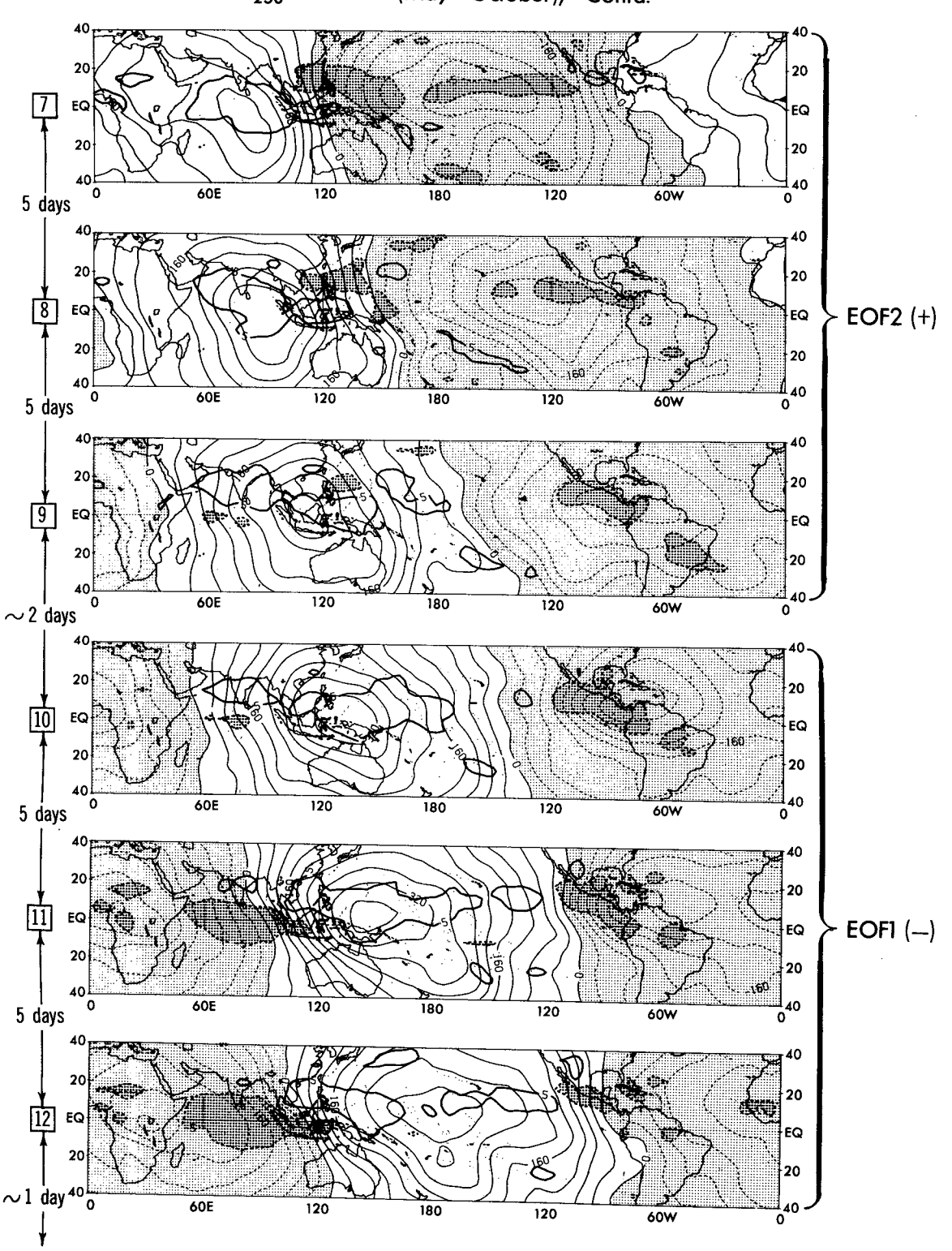

FIG. 8. (*Continued*)

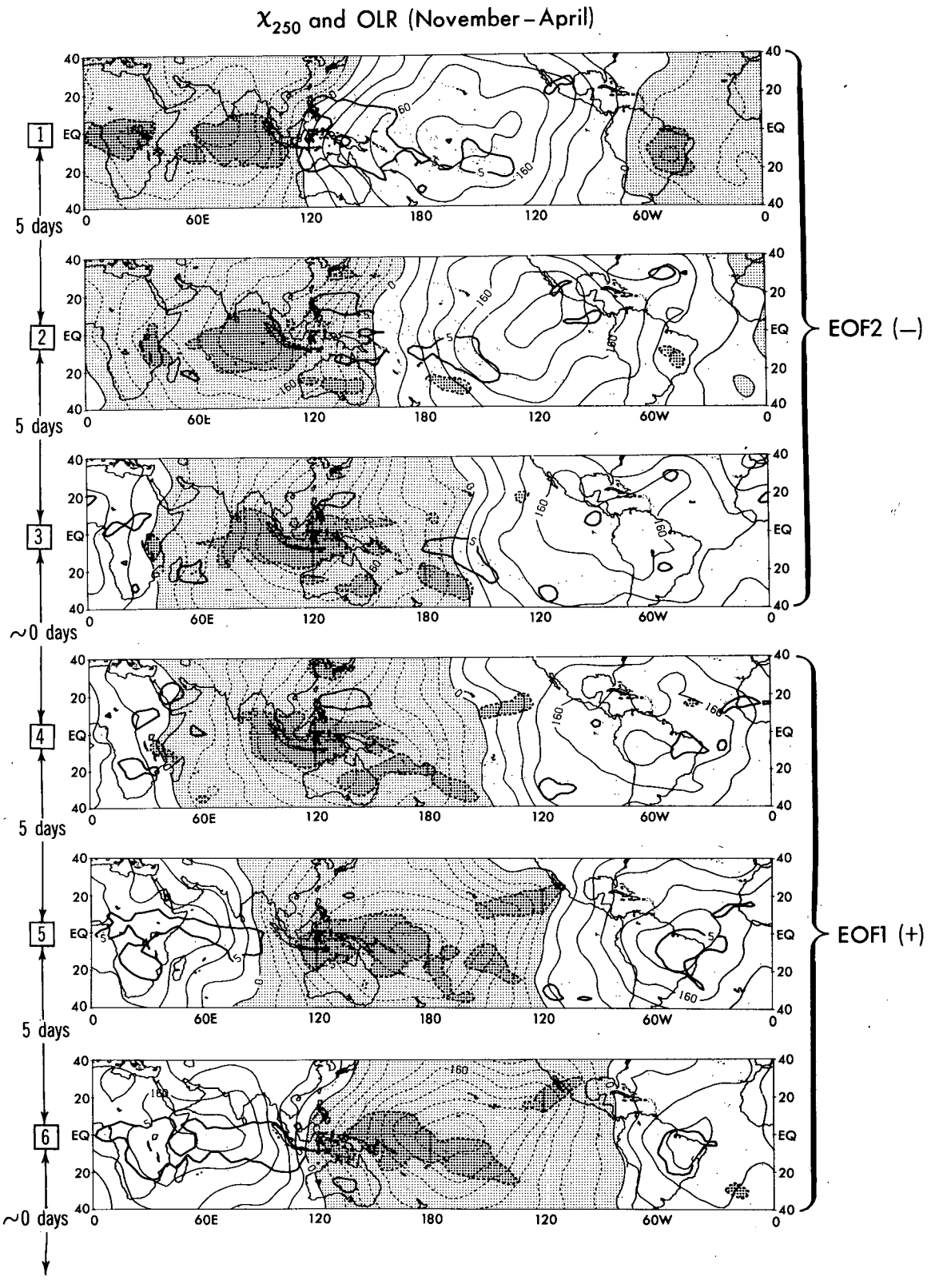

FIG. 9. As in Fig. 8 but for Northern Hemisphere winter season.

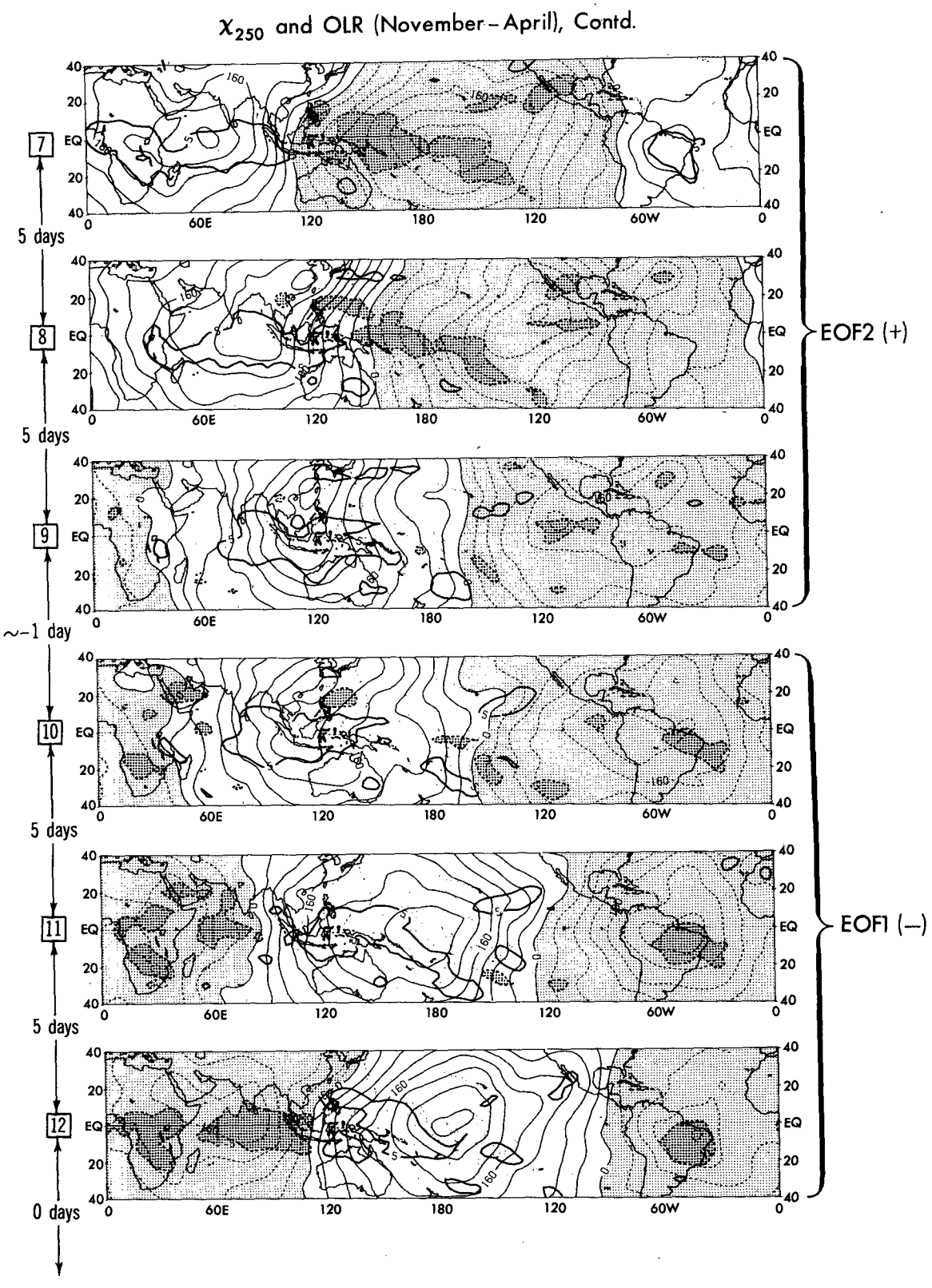

FIG. 9. (*Continued*)

and Africa (categories 8–12). The relative amplitude of composite OLR anomalies in different parts of the tropics will be shown more clearly in the Hovmöller diagram discussion (section 3d).

The large convection anomalies along the equator in the Indian Ocean (category 1) propagate eastward to the western tropical Pacific and northward into the Indian monsoon region as the large-scale vertical motion anomaly continues its eastward progression (categories 2–5). In categories 6–10 convection increases in the eastern Pacific intertropical convergence zone and Central America while the formerly active monsoon conditions over India have been replaced by "break monsoon" conditions. In categories 10–12 a new convection anomaly forms in the equatorial Indian Ocean, accompanied by the arrival of upper-level divergent westerly anomalies from the east.

The difference in characteristic eastward propagation speed for the circulation and OLR anomalies is clearly evident in the composites. For example, OLR anomalies occur at 80°E in the equatorial Indian Ocean beginning around category 11. One-half life cycle later (category 5), the greatest OLR anomalies are located around 150°E in the western Pacific. Thus, in one-half life cycle, the wavenumber-1 χ pattern has propagated half way around the globe, while the most prominent OLR anomalies have been confined primarily to the region 60°E–150°E. During the remaining half of the life cycle (categories 6–11), the OLR anomalies exhibit a faster apparent propagation as the large-scale χ pattern moves over the eastern Pacific and Central America.

b. Northern Hemisphere winter season

Figure 9 shows the composite large-scale convection and vertical motion features for the November–April season. As with the Northern Hemisphere summer season a fairly consistent relationship exists between anomalies of inferred large-scale vertical motion and the tropical convective activity. This agreement is particularly noteworthy since the NMC winds and satellite-measured OLR are essentially independent measures of tropical convective activity.

In categories 1–4, a fairly extensive convection anomaly over the equatorial Indian Ocean propagates eastward to Indonesia and the South Pacific convergence zone (SPCZ), which stretches to the southeast from Indonesia and New Guinea in category 4. An eastward displacement of the SPCZ occurs in categories 5–7. When the convection anomaly reaches the dateline, it is centered south of the equator. Negative OLR anomalies north of the equator in the extreme eastern Pacific (categories 4–7) may be related to fluctuations in the subtropical jet in this region rather than tropical convective activity.

In categories 8–10, convection near the dateline decreases as new anomalies appear to the east over South America and Africa. While tropical wind anomalies have continued to propagate eastward over the eastern Pacific Ocean, the convective activity in the Southern Hemisphere does not penetrate past about 150°W. It seems likely that while atmospheric dynamics favor a continued eastward progression of convective activity, other factors, such as lower sea surface temperatures or descending motion associated with the climatological-mean Walker Circulation suppress any further convective development to the east.

Categories 9–10 show fairly weak positive convection anomalies in the tropics while Indonesia experiences strongly suppressed convective activity accompanied by large-scale sinking motion. The Indian Ocean region experiences a renewal of convective activity in categories 11–12 accompanied by convective anomalies over South America and Africa.

The differences in apparent propagation speed for the OLR and χ_{250} patterns are not as pronounced for the November–April life cycle as for the May–October one. Large OLR anomalies occur over a greater fraction of the eastern hemisphere during the northern winter season. In particular, while negative OLR anomalies during NH summer categories 11–5 are primarily confined to 60°–150°E, during NH winter categories 12–6 the negative OLR anomalies occur from tropical Africa to east of the dateline.

c. Comparison of Northern Hemisphere summer and Northern Hemisphere winter

A comparison of Figs. 8 and 9 shows that convection anomalies associated with the oscillation are typically centered on or north of the equator in the Northern Hemisphere summer and on or south of the equator in the Northern Hemisphere winter, presumably following the seasonal cycle of maximum incoming solar radiation. As a result, the Indian monsoon region, southeast Asia, Central America and Brazil all experience strong seasonal differences in convection anomalies, with the strongest anomalies occurring during their respective rainy seasons. For a discussion of the mean and variance fields of OLR for these seasons, the reader is referred to our earlier reports (WLK and KWK).

During the Northern Hemisphere summer, the velocity potential patterns are smooth, with maxima and minima found almost exclusively in the tropics. In contrast, during the Northern Hemisphere winter categories 2–4, large-velocity potential anomalies occur in subtropical and high latitude regions (not shown) of the Northern Hemisphere. Further study is needed to determine whether this difference between divergent circulations in the winter hemisphere extratropics is real or due to data quality.

The regions of major OLR fluctuations over the eastern hemisphere during each season are consistent

with the east–west dipole structures identified by Lau and Chan (1985, 1986) although their analyses did not extend over the entire tropical domain. Murakami et al. (1986) have interpreted the eastward-propagating OLR patterns as a combination of zonal wavenumber 1 and 2 fluctuations. Our composite results show that the OLR fluctuations identified in these studies are phase-locked to the global-scale eastward-propagating circulation anomalies identified by Lorenc (1984), Krishnamurti et al. (1985) and others.

Based on the composites in Figs. 8 and 9 and the above studies, the 30–60 day oscillation can be characterized during both seasons as a global-scale fluctuation of tropical circulation features accompanied by more localized occurrences of convection anomalies. In addition to the major regions of OLR variability over the Indian Ocean and western Pacific, some potentially important OLR fluctuations occur over parts of the western hemisphere (e.g., South America and Central America). OLR fluctuations in these remote regions are consistent with the cross-spectral results of WLK and KWK.

d. Composite Hovmöller diagrams

Composite tropical χ_{250}, OLR, 850 mb zonal wind (U850), 250 mb zonal wind (U250) and subtropical ψ_{250} life cycles are shown in category versus longitude format in Fig. 10 for both May–October (a)–(e) and November–April (f)–(j) seasons. To approximate an equal time spacing between the plotted categories, only the four primary categories (2, 5, 8 and 11) are displayed. The slanted dark solid line on each plot shows the approximate progression of the χ_{250} composite anomaly center for each season.

As noted previously, the χ_{250} anomalies (a, f) exhibit global-scale eastward propagation, while the OLR anomalies (b, g) have their maximum amplitude in the eastern hemisphere. OLR anomalies in the longitude sector 60° to 160°E (dashed line) propagate more slowly (7–8 m s^{-1}) than a wavenumber-1 signal, although small amplitude OLR anomalies throughout the tropics are consistent with a wavenumber-1 structure and indicate an apparent global-scale organization of convection anomalies.

The zonal wind anomalies at 850 mb and 250 mb (c, d, h, i) confirm that the upper and lower tropospheric zonal wind anomalies are out of phase in the tropics during the composite oscillation. The phase of the zonal wind anomalies is consistent with the χ_{250} anomalies, with the anomalous winds changing direction near the maxima and minima of the velocity potential anomalies. The subtropical (winter hemisphere 10°–30°) ψ_{250} anomalies (e, j) also show evidence for large-scale eastward propagation. The structure and evolution of these anomalies will be discussed further in the next section.

4. Tropical and subtropical nondivergent circulation features

a. Northern Hemisphere summer

In Fig. 11, 250 mb streamfunction (ψ_{250}) composites for the May–October season are shown, with OLR composite anomalies superimposed as in Fig. 8. Major circulation features are identified by *L* and *H*.

In relation to tropical convective activity, there is a tendency for upper-air lows to occur to the east (categories 1–6) while upper-air highs tend to flank or lag behind the convective activity. The patterns suggest a strong zonal wavenumber-1 component exists in the streamfunction composites, within which a number of smaller-scale circulation systems are embedded. In general, there is a tendency for eastward development or propagation of the wavenumber-1 component as the convective activity shifts eastward.

Comparison of the location and intensity of individual features between categories (e.g., the ψ_{250} anomalies over Australia) suggests that certain regions are characterized by fairly persistent streamfunction anomalies during the oscillation. Individual highs and lows have a tendency to develop and strengthen in certain preferred geographical locations, although there is also some evidence for eastward propagation of individual features. Categories 11 and 12 illustrate the locations of the major regions of development for the smaller-scale Southern Hemisphere features. Two preferred locations occur in the South Pacific, one over the Atlantic, one over the Indian Ocean, and a fifth one over Australia.

The Northern Hemisphere ψ_{250} anomalies are smaller and less organized. The major regions of development are located over the western Pacific and near the west coast of North America. In cases where large ψ_{250} circulation anomalies occur in both hemispheres, the flow is approximately symmetrical about the equator (e.g., in category 12, the symmetric highs along 120°W).

b. Northern Hemisphere winter

During the November–April season (Fig. 12) the strongest ψ_{250} anomalies occur north of the equator. As with the Northern Hemisphere summer season, there is a large wavenumber-1 component in the rotational circulation anomalies within which smaller-scale individual features are embedded. While many of the Southern Hemisphere features are difficult to trace from one map to the next, some of the Northern Hemisphere features (e.g., the large circulation feature in the Pacific sector) can be traced for more than half an oscillation.

There is evidence for development and decay of circulation anomalies in certain geographical locations (30°N, 60°E in categories 5–7) as well as indications of eastward propagation of major circulation features

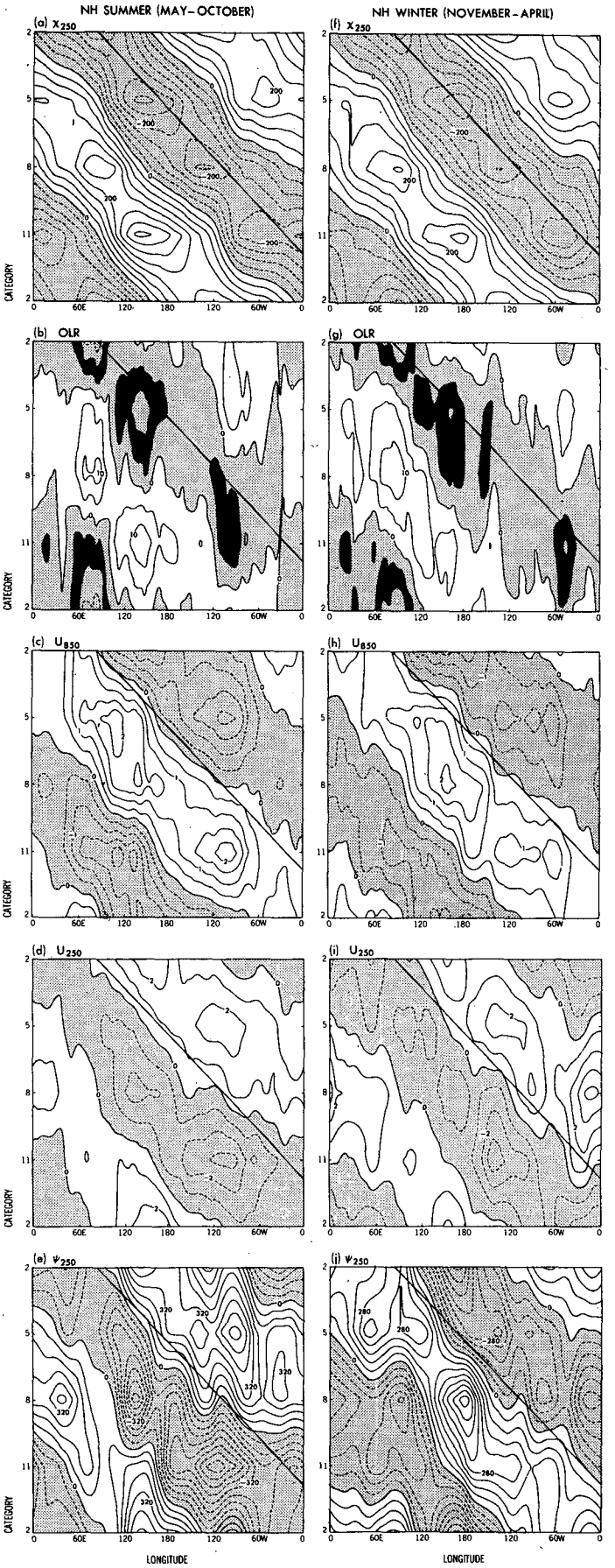
NH SUMMER (MAY–OCTOBER)
NH WINTER (NOVEMBER–APRIL)
(a) χ_{250}
(f) χ_{250}
(b) OLR
(g) OLR
(c) U_{850}
(h) U_{850}
(d) U_{250}
(i) U_{250}
(e) Ψ_{250}
(j) Ψ_{250}
CATEGORY
LONGITUDE
0 60E 120 180 120 60W 0
2 5 8 11 2

(in the north Pacific sector). The upper-air low in the north Pacific develops to the east of the strengthening convective activity, which is moving from the Indian Ocean to the dateline (categories 1–5). At the same time, an upper-air anticyclonic circulation develops in the Northern Hemisphere alongside the Indian Ocean convection (categories 1–2). By category 5 when the convection has reached 170°E, a broad region of anticyclonic circulations has formed over southern Asia. Category 6 shows that the upper-air low in the eastern Pacific has shifted east-northeast (30°N, 125°W), while a new cyclone has developed over western Africa. A high in the western Pacific sector straddles the decreasing convective activity over the dateline region (categories 6–9) and eventually reaches the eastern Pacific in association with the negative convection anomalies moving eastward out of the Indian Ocean (category 11).

The eastward progression of the wavenumber-1 pattern appears to result from a combination of in situ development and decay of smaller-scale features along with some instances of individual features propagating eastward. Evidence for symmetry of circulation features is limited but occurs, for example, in category 5 where the upper-air low in the eastern north Pacific has a cyclonic counterpart in the Southern Hemisphere.

The most prominent ψ_{250} features are the large cyclonic and anticyclonic circulations occurring in the Northern Hemisphere from Africa to the eastern Pacific. These features have a strong spatial association with the propagating tropical convective activity. The Pacific anomaly is particularly interesting because as it moves out over the Pacific it supports a fluctuation in the strength and eastward extension of the East Asian jet stream, as will be discussed later. Composite vector wind anomalies in this sector are about 7 m s^{-1} at 250 mb.

c. *Seasonal comparison*

A comparison of the composite ψ_{250} anomalies in Figs. 11 and 12 shows that the most prominent features occur in the Southern Hemisphere during the May–October season and in the Northern Hemisphere during the November–April season. In contrast, the OLR anomalies have a tendency to occur along the equator or in the Summer Hemisphere. Therefore, a characteristic of the oscillation's structure which occurs in both seasons is that the convection occurs preferentially in the Summer Hemisphere tropics while the strongest subtropical circulation anomalies accompanying the convection occur in the winter hemisphere.

5. Extratropical circulation features

Observational (e.g., Horel and Wallace, 1981) and modeling (Lau, 1985) studies have shown that sea-surface temperature anomalies in the tropics are associated with midlatitude circulation anomalies on interannual time scales. In contrast, the influence of the tropical 30–60 day oscillation on intraseasonal midlatitude variability is less clear. In this section, we investigate the links between the eastward-propagating tropical/subtropical features described in the previous two sections and the associated fluctuations of the extratropical circulation.

Weickmann (1983) and WLK have shown evidence that 30–60 day midlatitude circulation features are associated with 30–60 day tropical OLR oscillations during NH winter. Their results are extended in the present study by compositing extratropical 250 and 850 mb winds relative to tropical indices, testing statistical significance using Monte Carlo techniques, and examining the Northern and Southern Hemispheres for both May–October and November–April seasons. Lau and Phillips (1986) have performed a similar study using tropical OLR and 500 mb geopotential heights for the Northern Hemisphere winter.

The Monte Carlo testing procedure (see the Appendix) consisted of comparing the area-weighted percentage of wind vectors passing at t-test for each composite map to a statistical distribution of percentages generated using a randomized 30–60 day compositing procedure. When the percent of area passing the test for a given latitude domain exceeded the 95th percentile of the randomly generated distribution, the composite map was assumed to be "globally" significant over that latitude domain.

The test results for tropical (20°N–20°S) OLR and extratropical (25°–85°) vector winds are presented in Table 1. The tropical OLR composites are statistically significant (95%) throughout the life cycle in both seasons. The 250 mb and 850 mb vector winds in the tropics (results not shown) are also statistically significant in all categories for both seasons.

The extratropical vector winds for each season were tested separately for each hemisphere to reduce positive biasing of the results by highly significant tropical wind anomalies and to allow a separate test of the summer and winter hemispheres. The test results in Table 1 for the extratropics lead to the following conclusions:

1) The globally significant extratropical response is confined to the winter hemisphere during both May–October and November–April.

FIG. 10. Composite 30–60 day anomalies displayed in longitude vs category (time) format for May–October (a–e) and November–April (f–j). The variables plotted, contour intervals, and latitude region averaged are as follows: (a) χ_{250}, 5.0×10^5 m^2 s^{-1}, Eq–10°N; (b) OLR, 5 W m^{-2}, Eq–10°N; (c) 850 mb zonal wind, 0.5 m s^{-1}, Eq–10°N; (d) 250 mb zonal wind, 1.0 m s^{-1}, Eq–10°N; (e) ψ_{250}, 5.0×10^5 m^2 s^{-1}, 10°S–30°S; (f) χ_{250}, 5.0×10^5 m^2 s^{-1}, Eq–10°S; (g) OLR, 5 W m^2, Eq–10°S; (h) 850 mb zonal wind, 0.5 m s^{-1}, Eq–10°S; (i) 250 mb zonal wind, 1.0 m s^{-1}, Eq–10°S; (j) ψ_{250}, 5.0×10^5 m^2 s^{-1}, 10°N–30°N. Negative values are shaded. Further explanation of superimposed features is given in the text.

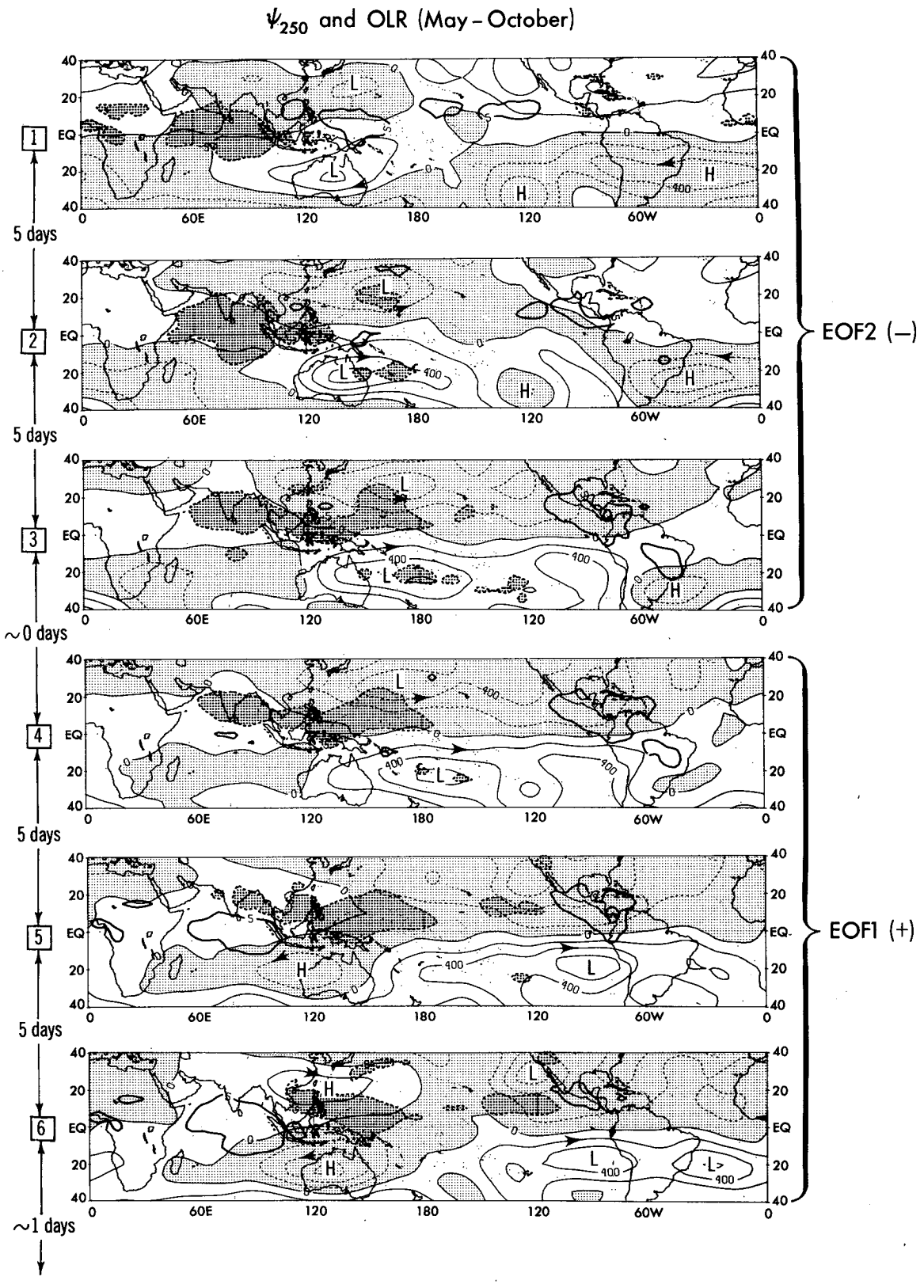

FIG. 11. Northern Hemisphere summer composite ψ_{250} anomalies (light contours, negative values have light shading) with superimposed OLR anomalies of at least 5 W m^{-2} in magnitude (dark contours, negative values have dark shading). Contour interval of ψ_{250} is 2.0×10^6 m^2 s^{-1}. The *L* and *H* denote cyclonic and anticyclonic circulation centers.

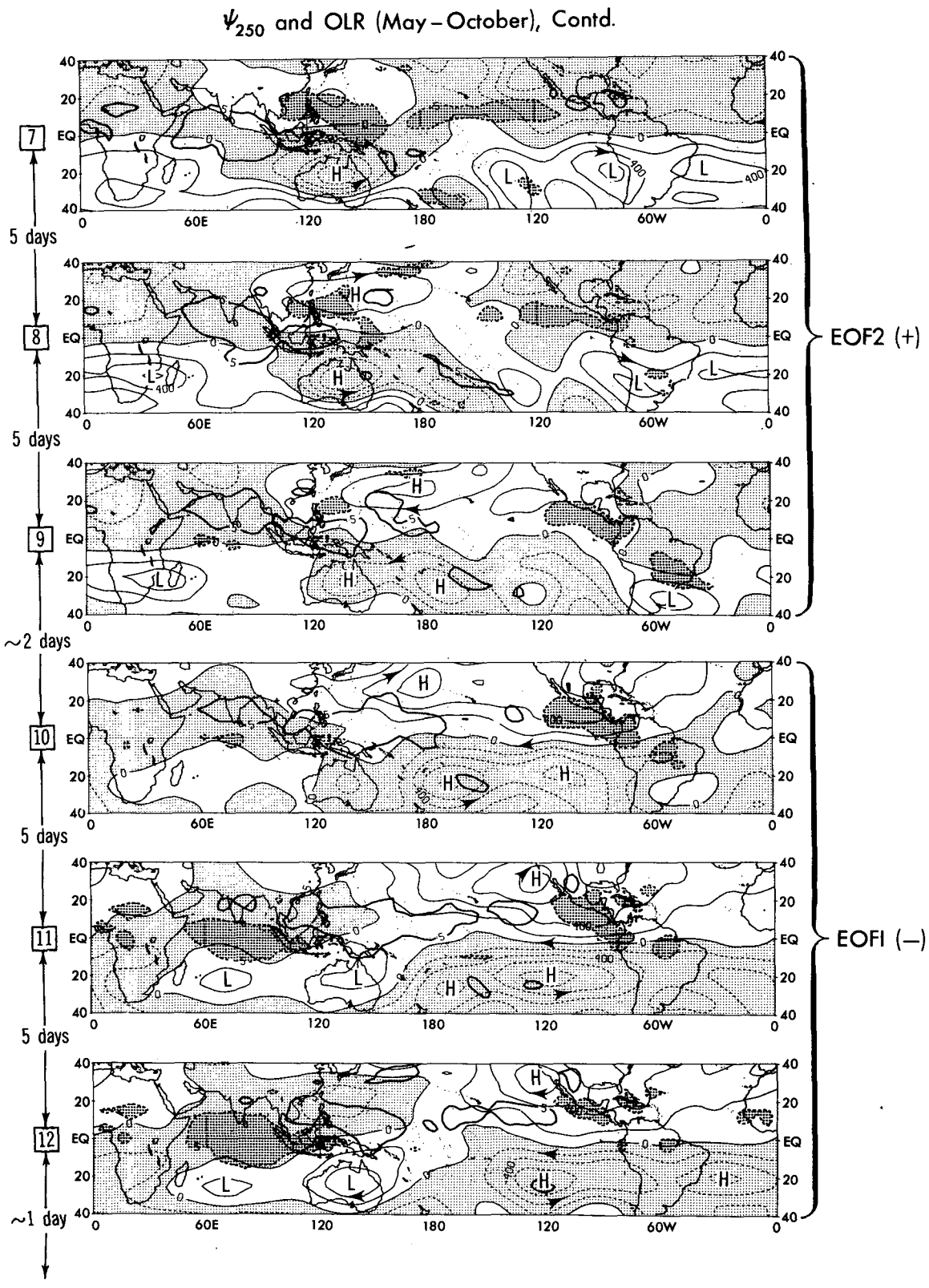

FIG. 11. (*Continued*)

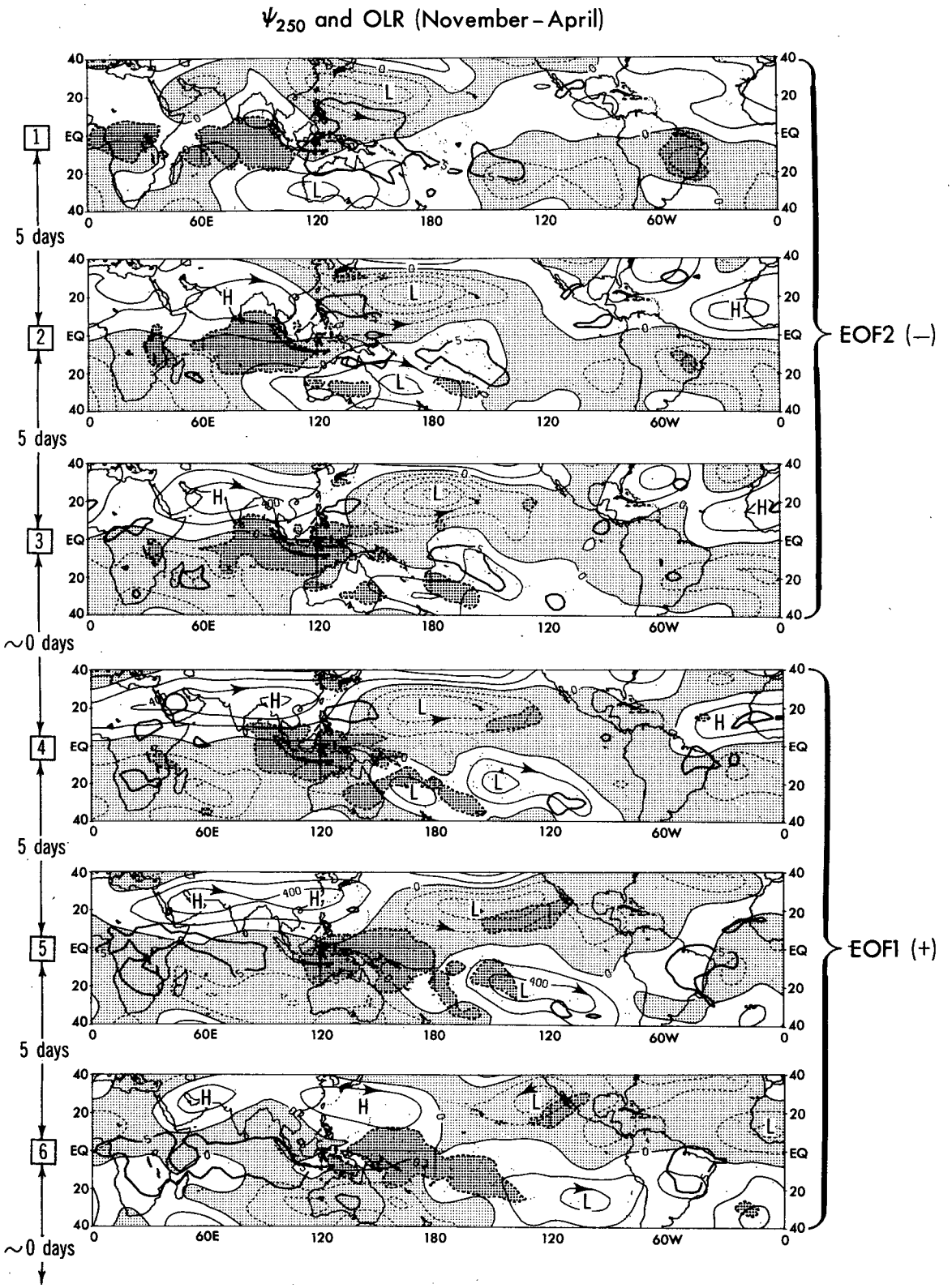

FIG. 12. As in Fig. 11 but for Northern Hemisphere winter season.

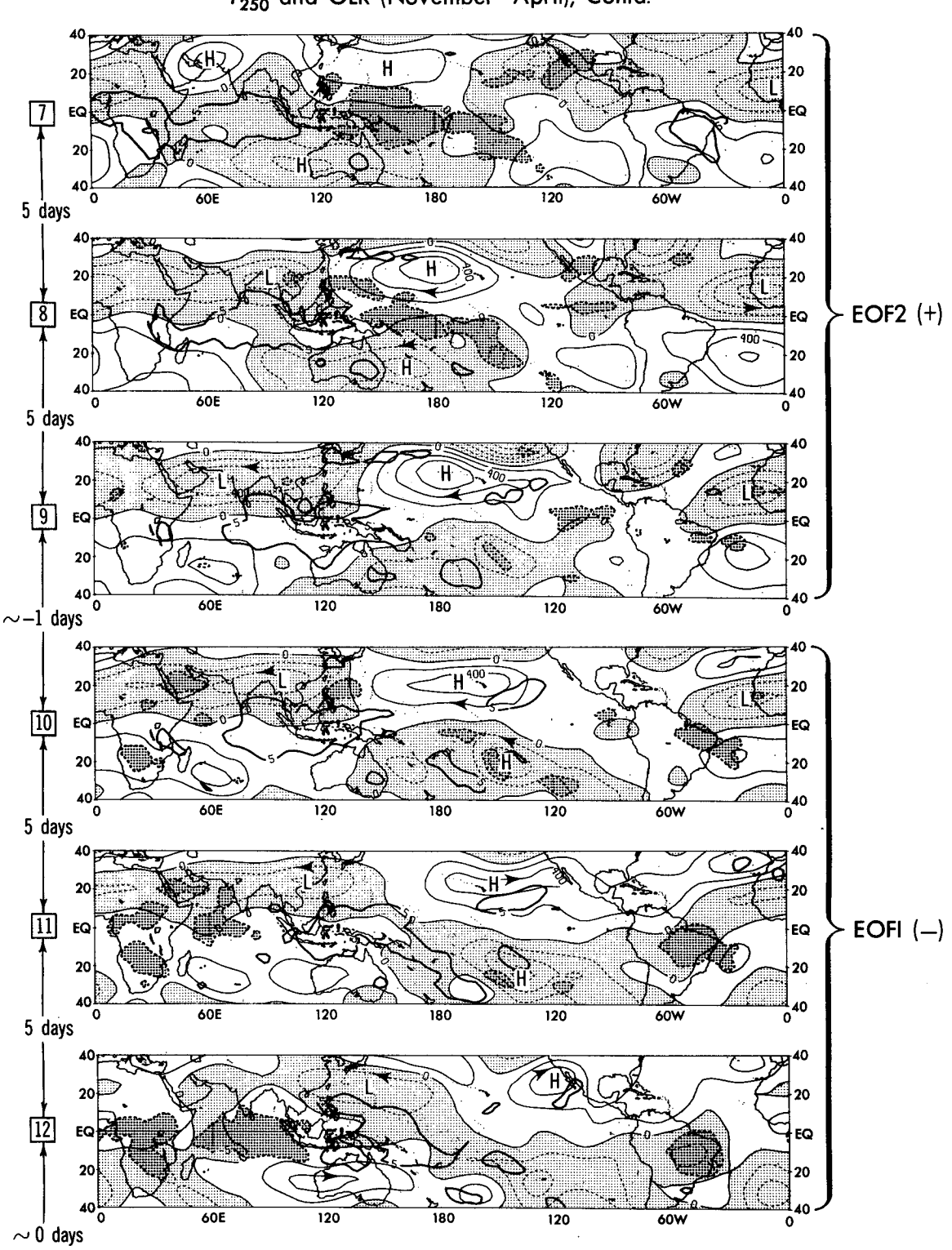

FIG. 12. (*Continued*)

TABLE 1. Fraction of area exceeding the 99% significance level. Fractions which meet the global significance criterion at the 95% (99%) level are indicated by *underlined* (*boldface*) numbers. Global significance criteria are based on statistics from 1000 randomly generated composites (see Appendix A).

Category	Number of pentads	OLR 20°N–20°S	V_{850} 25°N–85°N	V_{850} 25°S–85°S	V_{250} 25°N–85°N	V_{250} 25°S–85°S
(a) May–October						
1	17	.10	.03	.06	.03	.04
2	17	.09	.02	.07	.01	.07
3	17	.10	.03	.03	.01	.04
4	20	.12	.01	.03	.00	.02
5	20	.15	.02	.01	.01	.00
6	20	.15	.02	.11	.02	.10
7	16	.13	.02	.14	.01	.12
8	16	.07	.03	.16	.03	.17
9	16	.09	.04	.05	.02	.04
10	14	.09	.01	.01	.01	.00
11	14	.13	.01	.03	.01	.02
12	14	.13	.03	.05	.02	.03
Fraction needed for "global" significance:						
(95%)	~18/trial	.04	.08	.09	.08	.09
(99%)	~18/trial	.06	.11	.14	.12	.16
(b) November–April						
1	16	.09	.08	.02	.08	.00
2	16	.07	.11	.01	.10	.01
3	16	.06	.06	.02	.08	.01
4	15	.05	.05	.04	.09	.01
5	15	.07	.03	.07	.06	.03
6	15	.10	.05	.02	.02	.01
7	14	.07	.11	.02	.08	.00
8	14	.06	.14	.02	.16	.01
9	14	.05	.09	.04	.16	.01
10	14	.07	.05	.03	.09	.01
11	14	.08	.02	.03	.04	.03
12	14	.09	.06	.02	.03	.06
Fraction need for "global" significance:						
(95%)	~18/trial	.04	.09	.08	.09	.09
(99%)	~18/trial	.06	.12	.11	.13	.12

2) The greatest areal coverage of significant extratropical wind vectors occurs in category 8 during both half-years. In some cases, categories adjacent to category 8 are also statistically significant.

3) A secondary maximum in areal coverage occurs in category 2 for both half-years. However, category 2 is not globally significant for the May–October season.

4) Reference to Figs. 8 and 9 shows that the greatest extratropical "response" (~ category 8) occurs ~10 days after peak convective activity occurs over the western tropical Pacific during both seasons. Suppressed convective activity is indicated over the Indian Ocean at this time.

In Figs. 13 and 14, vector wind composites for categories 2 and 8 are displayed for the November–April and May–October seasons, respectively. May–October category 2, although not globally significant, is shown for comparative purposes. The lightly shaded regions on these maps show the locations of locally significant (99%) wind vectors in the *extratropics*. Asterisks on the arrow shafts also indicate local significance (99%) and are plotted in both the tropics and extratropics. The dark shading and contours denote OLR anomalies as in Figs. 8 and 9.

a. November–April

The composite 250 and 850 mb windfields for NH winter category 2 (average of 16 pentads) and 8 (14 pentads) are shown in Fig. 13 (a–d). According to these composites, the most prominent extratropical features accompanying the 30–60 day fluctuations of tropical convection are a series of cyclonic and anticyclonic circulation features over Asia and the North Pacific. These anomalies are pronounced at both 850 and 250 mb. The orientation of these features is suggestive of an extratropical wavetrain, although the physical link to the anomalous tropical convection is not as obvious as with the idealized model solutions of Hoskins and Karoly (1981). In general, the vectors in category 8 (both 250 and 850 mb) are oriented opposite to the category 2 vectors.

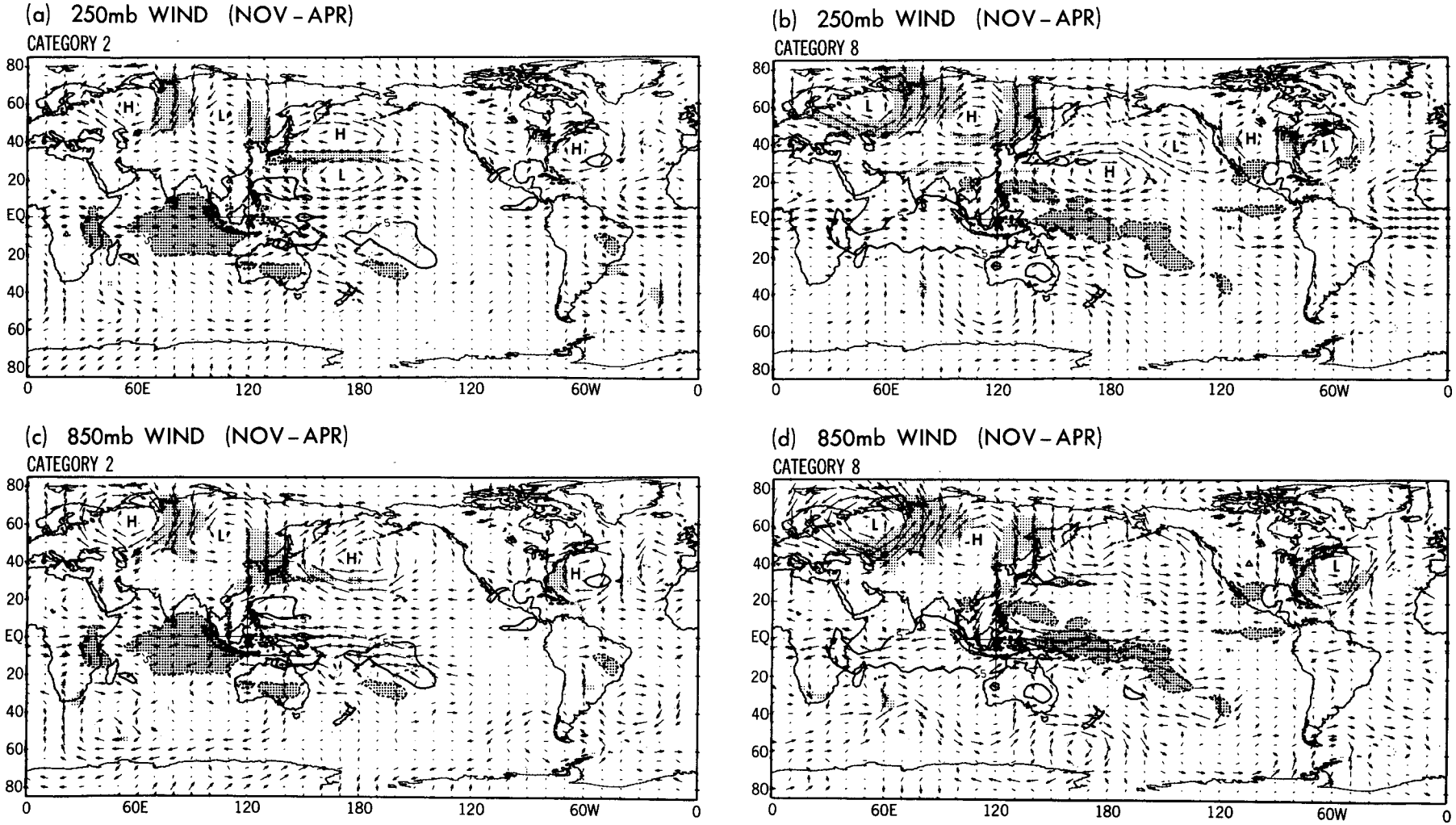

FIG. 13. Northern Hemisphere winter global vector wind composites for (a) Category 2, 250 mb; (b) Category 8, 250 mb; (c) Category 2, 850 mb; (d) Category 8, 850 mb. OLR anomalies are superimposed as in Fig. 9. Asterisks indicate vector anomalies significant at the 99% level. Light stipple outlines significant regions for the extratropics (25°–85°) of both hemispheres. Maximum wind anomalies shown are ~8 m s^{-1} (250 mb) and ~4 m s^{-1} (850 mb).

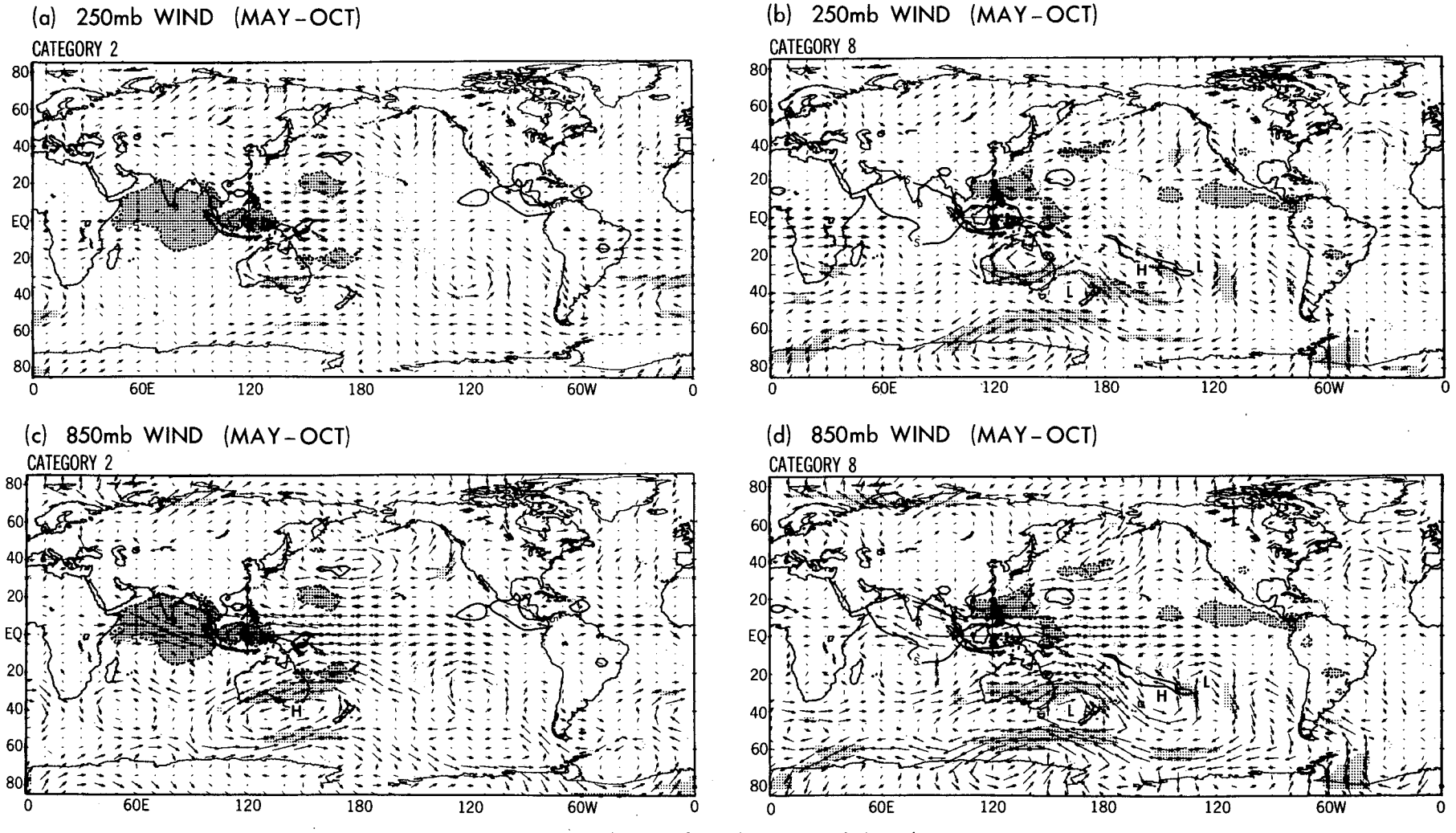

FIG. 14. As in Fig. 13 but for the Southern Hemisphere winter.

One possible region of tropical-extratropical interaction is along the east coast of Asia, where the 850 mb composites for both categories 2 and 8 (Fig. 13c, d) show statistically significant meridional flow connecting tropical and extratropical regions. For example, in category 8, anomalous 850 mb northerly flow extends along the east coast of Asia from 70°N to the equator where it joins with tropical westerly and easterly anomalies associated with the anomalous tropical convection. Weaker low-level meridional flow occurs off the east coast of North America during categories 2 and 8 in association with an anomalous circulation feature over the western Atlantic.

In relation to the tropical convection, the composites indicate that anomalous *southerly* flow along the east coasts of Asia and North America occurs at a time of anomalous convective activity over the equatorial Indian Ocean. The movement of anomalous tropical convective activity to the western Pacific is followed by anomalous *northerly* flows in these locations. These statistically significant meridional flows off the east coast of Asia may indicate a dynamical link between the tropical and extratropical circulation features in this region.

The 250 mb composite for category 2 indicates highly significant zonal wind fluctuations near the exit region of the East Asian Jet (EAJ) along with the previously noted circulation features over Asia. In terms of synoptic features, the EAJ is retracted westward toward Asia when tropical convection is strong over the equatorial Indian Ocean. As the convection anomalies move eastward to the western and central Pacific (category 8) the EAJ extends eastward toward North America. Most of the anomalies associated with this extension are locally significant at the 95% level. In the North American sector (category 8) some less pronounced but statistically significant circulation features are found.

Over the tropical western Pacific (10°N–30°N; 120°E–150°E), southerly upper-level flow occurs on the western edge of a large anticyclonic circulation (category 8). The southerly flow at 250 mb, combined with the previously noted northerly flow at 850 mb, is suggestive of an anomalous local meridional mass circulation. Evidence for these features can also be found (of opposite sign) in category 2.

A comparison of the 850 mb (a, b) and 250 mb (c, d) vectors indicates that in the tropics (20°N–20°S) vector wind anomalies tend to be out of phase between these two levels, while in the extratropics, anomalous winds are approximately in phase (equivalent barotropic). Consistent with this latitudinally varying vertical structure is a prominent cyclonic (anticyclonic) circulation anomaly which occurs near 25°N, 170°E in category 2 (8) of the *250* mb composites but is absent in the *850* mb composites.

b. May–October

The most prominent extratropical circulation features accompanying the tropical convection oscillation during the southern winter (Fig. 14, a–d) are zonally elongated zonal wind perturbations over southern Australia and along 50°S–70°S. The anomalous westerlies over southern Australia, which are evident at 850 mb and 250 mb in category 8 (Fig. 14b, d) occur when convection is suppressed over the Indian Ocean and 5–10 days after peak convective activity occurs in the western tropical Pacific. The climatological-mean 250 mb vector wind field during May–October (e.g., Fig. 2a in KWK) shows a split-flow pattern with a strong jet along 25°–30°S over and to the east of Australia along with a weaker midlatitude jet along 60°S. The 250 mb composite anomalies in category 8 indicate that the Australian jet feature is strengthened at this time during an oscillation. Significant meridional wind fluctuations occurring over the South Pacific in category 8 (Fig. 14b, d) are suggestive of a "wavetrain" of circulation features.

The category 2 composites (Fig. 14a, c) contain many of the features noted for category 8, although the arrow directions are reversed, and the amplitudes and statistical significance are much lower. A comparison of the 250 and 850 mb composite vectors for categories 2 and 8 indicates that, in agreement with the November–April composites, the upper and lower tropospheric anomalies are in phase in the extratropics and out of phase over tropical regions.

c. Relation to previous work

Some aspects of the extratropical results for the November–April season are consistent with WLK's composite life cycle in which a transition from an expanded to contracted circumpolar vortex over the western hemisphere was highlighted. The differences which exist between the two composite life cycles may be related to the different compositing indices used. WLK's indices emphasized variability near the exit regions of the midlatitude jet streams, while our indices are more directly linked to tropical convective activity. Nevertheless, both life cycles include an eccentric circumpolar vortex pattern characterized by alternate weakening and strengthening of the East Asian and North American jet streams. In our composite life cycle, this pattern is most evident ~5 days after categories 2 and 8, although a contracted (expanded) vortex pattern over the Pacific Ocean and western hemisphere is already indicated in our category 2 (8). In contrast, the "wavetrain" over northern Asia in our categories 2 and 8 was less evident in WLK, possibly because it is best developed 5–10 days before the maximum intensification or weakening of the jet streams.

The sequence of circulation anomalies over Asia, the northern Pacific and North America (category 8) bears some resemblance to the wavetrain description given by Lau and Phillips (1986, compare their DAY 5 to our category 2). However, the positions of the centers of action are not coincident, and their Pacific/North American wavetrain is not well defined in our category 2. Differences in the filter (20–70 vs 30–60

days), data period, variables (500 mb heights vs 250/850 mb winds) and analysis approach may account for some of these discrepancies.

Lau and Lau (1986) have performed a similar analysis to the one described in this paper, using 25–40 day filtered output from a low-resolution GCM. One difference between their results and ours concerns the extratropical anomaly patterns which accompany the eastward-propagating χ anomalies. Lau and Lau obtained the greatest extratropical "response" at a time when the model velocity potential anomalies are nearly in quadrature with our category 2 and 8 anomalies. In addition, our composite extratropical patterns show more prominent anomalies in the Asian sector, while Lau and Lau's most prominent patterns emphasize the North American sector. A major point of agreement between our results and those of Lau and Lau is that the significant extratropical "response" occurs in the winter hemisphere.

6. Fluctuations of the Indian monsoon

An important aspect of the 30–60 day oscillation is its modulation of Indian monsoon convection during the Northern Hemisphere summer. Yasunari (1980, 1981), KWK, and others have described periodic northward-propagating convection anomalies in the summer monsoon region while Krishnamurti and Subrahmanyam (1982), Krishnamurti et al. (1985), and others have described fluctuations in the monsoon circulation on this time scale.

The composite relationship between the convection, 850 mb NMC vector wind anomalies and the propagating χ_{250} pattern is illustrated in Fig. 15 (northern summer categories 1–6). The composites show a northward-propagating cyclonic circulation feature accompanying the northward-propagating convective activity in the Indian monsoon region. The climatological-mean Somali jet is similar in structure to the anomalies in category 4; thus, the anomalies in categories 3–6 show that the strength of the jet is modulated during an oscillation.

In categories 5 and 6, the positive convection anomalies are decreasing over India as anomalously clear or "break monsoon" conditions begin to occur. The composite structure on this regional scale appears reasonable even though we used global-scale features of the 250 mb wind field as a composite basis; this result confirms the strong statistical link between monsoon convection in 30–60 day time scales and the global-scale eastward-propagation χ_{250} "wave". Our composite method shows the larger-scale structure of 850 mb vector wind anomalies in this region. The filtered (not composited) maps of Krishnamurti and Subrahmanyam (1982) for the Northern Hemisphere summer 1979 have shown that embedded within this large-scale pattern are individual synoptic disturbances.

7. Discussion and concluding remarks

Using empirical orthogonal function analysis of 30–60 day filtered 250 mb velocity potential as a compositing basis, we have examined the life cycle of the 30–60 day oscillation in tropical convection, large-scale tropical divergent and rotational circulations, and extratropical vector winds for both the May–October and November–April seasons.

Tropical convection (OLR) and large-scale divergent circulation (χ_{250}) patterns show a coherent eastward-propagating structure for both seasons. Large-amplitude OLR fluctuations over the eastern hemisphere are phase-locked to the global-scale eastward-propagating χ_{250} "wave", with the largest OLR anomalies exhibiting a slightly slower eastward progression, particularly during May–October. To the east of the convection anomalies, anomalous upper-air cyclonic circulations in the winter hemisphere subtropics are evident, with anticyclonic circulations occurring to the west or alongside the convection. Modulation of the Indian summer monsoon convective activity on 30–60 day time scales is temporally associated with the passage of the large-scale divergent circulation pattern during the May–October season.

Some statistically significant associations were found between midlatitude circulation anomalies in the winter hemisphere and the fluctuating tropical convective activity. For example, during northern winter the East Asian jet is retracted toward Asia when strong convection is occurring over the equatorial Indian Ocean. The eastward progression of anomalous convection into the western and central Pacific is accompanied, in the composite oscillation, by the occurrence of a series of circulation features over Asia and an eastward extension of the East Asian jet. During southern winter, the jet over southern Australia is anomalously strong about 10 days after peak convective activity occurs in the tropical western Pacific.

Preliminary examination of the oscillation's vertical structure, based upon 12 levels of NMC χ data and composite zonal winds, revealed a reversal in wind anomaly direction between upper and lower levels in the tropics, with coherent lower-level anomalies from 1000 to 500 mb and coherent upper-level anomalies over the region 250–100 mb. Poleward of 20°, vector wind anomalies indicated little phase shift between the 250 and 850 mb levels.

The composite life cycles presented in this study may provide some insight into the fundamental nature of the oscillation. Our results demonstrate that large-scale features of the tropical divergent wind field propagate eastward around the globe once per oscillation, accompanied by anomalous convective activity in many regions. This behavior occurs in both seasons, in contrast to some other characteristics of the oscillation (e.g., modulation of the Indian summer monsoon or association with Northern Hemisphere extratropical patterns) which are seasonally dependent.

Recently, Lau and Lau (1986) have shown that χ anomalies propagate eastward around the globe in long-term integrations of a GFDL GCM. Their 25–40 day composite oscillation is similar in many respects to our observed composite life cycle, particularly over the

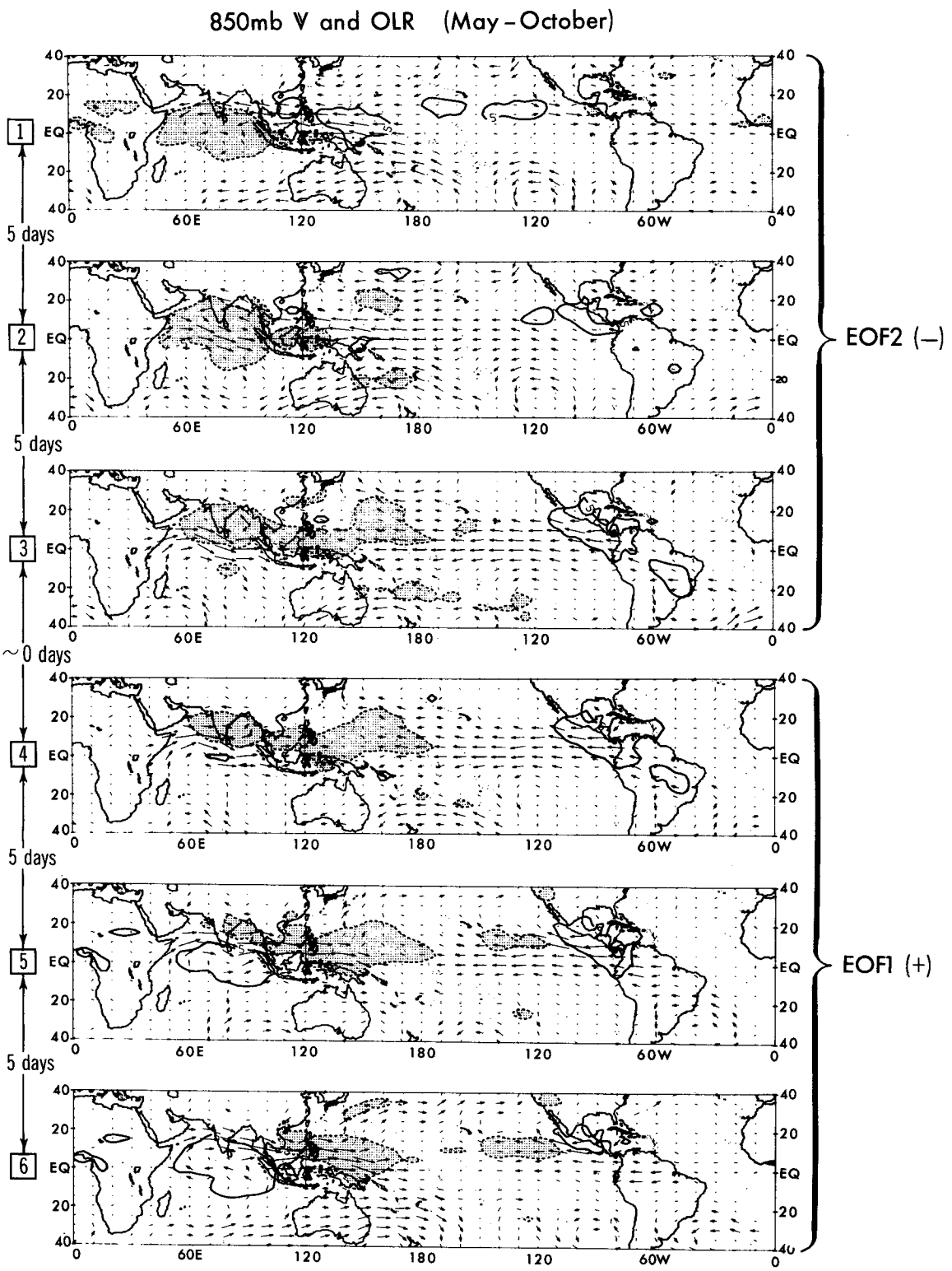

FIG. 15. 850-mb vector wind composites (categories 1–6, 40°N–40°S) during Northern Hemisphere summer, with OLR anomalies superimposed as in Fig. 8. The maximum wind anomaly is about 4 m s^{-1}.

tropics. For example, composite vector wind anomalies in the tropics are dominated by the zonal component in both the observed (e.g. Figs. 13, 14, 15) and modeled oscillations, and both modeled and observed oscillations show northward-propagating convection anomalies in or near the Asian summer monsoon region.

Hayashi and Sumi (1986) have studied 30–40 day oscillations in a GCM for an ocean-covered earth. Their results show that model precipitation and zonal wind anomalies have a large eastward-propagating wavenumber-1 component. They attribute the eastward propagation to wave-CISK convergence processes and the wavenumber-1 zonal structure to the effects of convection-suppressing downdrafts occurring in a finite (periodic) longitudinal domain.

While the time scale of the oscillation in their model is determined by the time required for the large-scale convection/circulation wave to propagate around the globe, our composite results for the real world show that convection (OLR) anomalies associated with the χ_{250} "wave" are very weak over many parts of the tropics. This implies that the coupled convection/circulation mode identified by Hayashi and Sumi would not be expected to occur uniformly over all longitudes of the tropics (e.g., warm vs cool sea surfaces; ocean vs land). Furthermore, since there are periods of strong oscillations followed by more quiescent periods (e.g., early 1981, spring 1983 and early 1984 in Fig. 3), a generation mechanism not necessarily related to the previous oscillation may often be important.

Nevertheless, the characteristic global-scale eastward propagation of χ anomalies, which is present throughout the seasonal cycle in the observations and in numerical simulations, may be important for producing the observed oscillation's time scale. One possibility is that each new event is initiated by remnants of the previous oscillation approaching from the west. The smaller convection anomalies over the Central/South American sector could act to rejuvenate the oscillation after it has traveled over cooler sea surfaces. Another possibility is that a new oscillation can begin once the convection-suppressing influences (subsidence, low-level moisture divergence, etc.) of the previous event have moved "far enough" away to the east. While our results show a consistent spatial association between the transient χ_{250} and OLR patterns, it is still unclear whether circulation anomalies propagating eastward around the globe initiate new episodes of convective activity.

A recent modeling study by Anderson and Stevens (1986) provides an alternative interpretation of our composite results. Using a fully stratified tropical model which included cumulus friction and a Hadley cell basic-state circulation, they show that some eastward propagation of tropical circulation features can occur even when the anomalous heating remains fixed in one location. From this viewpoint, the convection anomalies occurring over the Indian Ocean and western Pacific could be forcing an eastward-propagating global-scale response in the tropical circulation. Anderson (1984) further suggests that oscillations on the 40–50 day time scale can result from processes associated with the Hadley circulation, without requiring a global-scale eastward propagation of atmospheric anomalies.

Regardless of the fundamental mechanism producing the model time scale, the physical process causing the eastward shifts of OLR anomalies in the Indian Ocean and western Pacific regions remains uncertain. Although the dynamical processes identified in the modeling study of Hayashi and Sumi (1986) may play a significant role, an examination of other variables, such as moisture, precipitation, SST and surface heating, in both observations and models, may be necessary to provide a final explanation.

The subtropical ψ_{250} circulation features at upper levels in our composites (Figs. 11 and 12) are reminiscent of Webster's (1972, Fig. 9) two-layer model results for a localized, steady equatorial heating anomaly. For example, Webster's model shows 250 mb cyclonic flow east of the heating and anticyclonic flow to the west with symmetry of circulation features about the equator. Madden (1986) has provided an additional, more detailed description of the observed atmospheric response to large-scale 40–50 day tropical heating anomalies.

The coarse features of the oscillation's extratropical vertical structure are consistent with the modeling studies of Hoskins and Karoly (1981), who noted an equivalent barotropic structure away from the region of thermal forcing, and the GCM composites of Lau and Lau (1986). While the oscillation's vertical structure clearly varies with latitude, the detailed height–latitude structure and the physical mechanisms determining the "transition latitude" for the vertical structure requires further study.

With respect to extratropical fluctuations, our composite results show statistically significant temporal relationships on 30–60 day time scales between tropical convection anomalies and circulation patterns in the winter hemisphere extratropics. These circulation patterns are more complicated than the idealized wavetrain patterns modeled by Hoskins and Karoly (1981) for a steady forcing.

The differences between the Northern and Southern Hemisphere wintertime anomaly patterns and the differences between the summer and winter hemisphere extratropical response are both suggestive of the important role of the extratropical basic state circulation on tropical–extratropical interactions. The model results of the Simmons et al. (1983) and Branstator (1985) have indicated that the extratropical base state circulation is an important factor in determining the midlatitude response to a tropical forcing. The occurrence of large wind anomalies in the exit region of the East Asian Jet in our composites is also reminiscent of their findings.

While the composite extratropical patterns discussed in section 5 have some interesting structure, their utility for long-range midlatitude weather forecasting is not known. Our results are limited by the fact that we have

used only six years of data, and that the compositing procedure we have used is based primarily upon the tropical divergent circulation. The true extratropical response may vary greatly from event to event, depending on such factors as the location, amplitude, and persistence of the tropical heating anomaly and the existing extratropical circulation. The use of 6-month seasons could also lead to an underestimate of the strength of the wintertime remote response since the fall and spring basic states are significantly different from the December–February state. An explanation of the dynamical mechanisms producing the extratropical/tropical link will require further investigation of both observed and modeled data.

Our synoptic experience with observing individual cases suggests that the connections described by our composite maps are well-developed in one or two individual cases during a typical winter. The persistence of the resulting expanded or contracted vortex patterns also varies from case to case; the tropical oscillations may be more effective in producing transitions of the extratropical circulation than in causing the persistence of a given pattern.

In summary, the composite life cycles presented in this study show the time evolution of the anomalous convective activity and global-scale circulation features associated with the tropical 30–60 day atmospheric oscillation. Based upon these results, a number of fundamental questions about the oscillation are posed:

- Does the time scale result from global-scale eastward propagation as suggested by the results of this study?
- Why do the observed circulation and convection anomalies propagate eastward and what determines the propagation speed?
- What is the role of the eastward-propagating equatorial Kelvin waves and the "coupled Kelvin–Rossby modes" (Hayashi and Sumi, 1986) in the observed oscillation?
- What determines the "transition latitude" where the vertical phase difference between the 850 and 250 mb composite wind anomalies changes?
- How important is the effect of the 30–60 day oscillation on the extratropical circulation and what physical mechanisms are important for producing the extratropical response?

Possible answers to these questions have been given in a number of recent modeling studies; however, further studies of low-frequency variability in general circulation models (GCMs) are planned, including comparisons between observed and modeled oscillations. These studies may provide an explanation for the eastward propagation of χ anomalies in the GCMs (e.g. Lau and Lau, 1986) and for the fundamental time scale of the model oscillation. If the model dynamics accurately reproduce the fundamental mechanisms of the observed phenomenon, these studies may provide a dynamical basis for understanding the 30–60 day oscillations in the real world.

The practical importance of the oscillation for extended-range weather forcasting remains undetermined, although certain regions of the world (e.g., tropical latitudes) are likely to realize a greater forecasting improvement. Rainfall prediction, statistical forecasting of tropical cyclone activity and improved extended-range global forecasts by refined general circulation models are areas in which the oscillation might have predictive utility.

Acknowledgments. This research was partially supported by NOAA Grant NA-79AA-D-00129 and by NSF Grant ATM82-19079 at the Center for Climatic Research, University of Wisconsin—Madison. We thank J. Kutzbach, R. Pierrehumbert, N.-C. Lau and an anonymous reviewer for useful suggestions; J. Pege and W. Marshall for typing the manuscript; J. Connor for photography; and the GFDL technical illustrations group for drafting the figures. Lau kindly provided the bandpass filter used in this study.

APPENDIX

Statistical Significance Tests

The statistical significance of the composite maps was assessed by calculating the percent area (cosine-weighted by latitude) passing a local t-test at a given significance level (Level 1 test). This value was compared to a frequency distribution of percent area passing the same test applied to 1000 randomly generated composite maps following Livezey and Chen (1983). The 95% level was chosen for the final test phase (Level 2) which meant that in order for a composite map to be significant, the percent area passing the Level 1 test had to exceed the 95th percentile of the randomly generated distribution.

The appropriate level for the initial tests (Level 1) depends somewhat upon the type of features one wishes to highlight. Because of the relatively small spatial coverage of OLR anomalies in relation to the overall tropical domain, the 99% level was used for all variables along with a number of simplifying assumptions which were duplicated in the Monte Carlo simulations.

The first assumption was that the observations used in each composite map were temporally independent. In order to duplicate this feature in the Monte Carlo tests, the random composites were constructed in the same manner as the actual composites (section 2d) except that random 30–60 day basis series were used to select dates rather than the χ_{250} principal component series. The random 30–60 day series were generated by applying a 30–60 day filter to normally distributed random input series. Thus, the basis series and datasets being composited had similar spectral and autocorrelation characteristics (temporal degrees of freedom) for both the actual tests and the simulated tests. The second assumption was that if either the u or v component of the vector wind was found to be significant, the vector quantity was assumed significant. The simulated tests were done the same way.

The effects of spatial degrees of freedom were included in the results because identical datasets and latitude domains were used in forming the composites for both the actual significance tests and the simulations. As the number of spatial degrees of freedom decreased (e.g., for limited latitude domains or variables with larger characteristic spatial scales) the frequency distributions became broader and the 95th percentile increased.

The statistical significance of variables was tested over certain a priori specified latitude domains. For example, since we were primarily interested in tropical fluctuations in convection, OLR results were tested over the domain 20°N–20°S. The tropical and subtropical vector windfields were tested over the domain 40°N–40°S. All tropical OLR composites (20°N–20°S) and 250 mb wind composites (40°N–40°S) were significant at the 95% level for both seasons.

In testing the significance of extratropical wind composites, we chose the latitude domain 25°–85° for each hemisphere (tested separately). Tropical latitudes, which were highly significant, were omitted to reduce positive biasing of the results. A separate Monte Carlo simulation of 1000 cases was performed for each season. The results of the tests are summarized in Table 1 (see section 5).

REFERENCES

Anderson, J. R., 1984: Slow motions in the tropical troposphere. PhD. thesis, Colorado State University, Atmos. Sci. Paper No. 381, 144 pp.

——, and D. E. Stevens, 1986: The response of the tropical atmosphere to low-frequency thermal forcing. *J. Atmos. Sci* (in press).

——, —— and P. R. Julian, 1984: Temporal variations of the tropical 40–50 day oscillation. *Mon. Wea. Rev.*, **112,** 2431–2438.

Blackmon, M. L., R. A. Madden, J. M. Wallace and D. S. Gutzler, 1979: Geographical variations in the vertical structure of geopotential height fluctuations. *J. Atmos. Sci.*, **36,** 2450–2466.

Branstator, G., 1985: Analysis of general circulation model sea-surface temperature anomaly simulations using a linear model. Part I: Forced solutions. *J. Atmos. Sci.*, **42,** 2225–2241.

Climate Analysis Center, 1985: Climate Diagnostics Bulletin, Dec. 1985, Publ. NOAA/National Weather Service, National Meteorological Center, Washington, DC, 2–3.

Cooley, D. S., 1974: A description of the Flattery global analysis method—No. 1. *Tech. Proc. Bull. No. 105,* NWS, NOAA, U.S. Dept. of Commerce, 9 pp.

Goswami, B. N., and J. Shukla, 1984: Quasi-periodic oscillations in a symmetric general circulation model. *J. Atmos. Sci.*, **41,** 20–37.

Hayashi, Y.-Y., and A. Sumi, 1986: The 30–40 day oscillations simulated in an "aqua planet" model. *J. Meteor. Soc. Japan,* **64,** 451–466.

Horel, J. D., and J. M. Wallace, 1981: Planetary-scale atmospheric phenomena associated with the Southern Oscillation. *Mon. Wea. Rev.*, **109,** 813–829.

Hoskins, B. J., and D. J. Karoly, 1981: The steady linear response of a spherical atmosphere to thermal and orographic forcing. *J. Atmos. Sci.*, **38,** 1179–1196.

Knutson, T. R., K. M. Weickmann and J. E. Kutzbach, 1986: Global-scale intraseasonal oscillations of outgoing longwave radiation and 250 mb zonal wind during Northern Hemisphere summer. *Mon. Wea. Rev.*, **114,** 605–623.

Krishnamurti, T. N., and D. Subrahmanyam, 1982: The 30–50 day mode at 850 mb during MONEX. *J. Atmos. Sci.*, **39,** 2088–2095.

——, P. K. Jayakumar, J. Sheng, N. Surgi and A. Kumar, 1985: Divergent circulations on the 30–50 day time scale. *J. Atmos. Sci.*, **42,** 364–375.

Kutzbach, J. E., and K. M. Weickmann, 1984: The global distribution of the annual and semiannual cycles of outgoing longwave radiation and 250 mb *u*-component winds. In *Studies in Climate,* (H. van Loon, Ed.), NCAR Tech. Note NCAR/TN-227+STR, p. 44–64.

Lau, K.-M., and P. H. Chan, 1985: Aspects of the 40–50 day oscillation during the northern winter as inferred from outgoing longwave radiation. *Mon. Wea. Rev.*, **113,** 1889–1909.

——, and ——, 1986: Aspects of the 40–50 day oscillation during the northern summer as inferred from outgoing longwave radiation. *Mon. Wea. Rev.*, **114,** 1354–1367.

——, and T. Phillips, 1986: Coherent fluctuations of extratropical geopotential height and tropical convection in intraseasonal time scales. *J. Atmos. Sci.*, **43,** 1164–1181.

Lau, N.-C., 1985: Modeling the seasonal dependence of the atmospheric response to observed El Niños in 1962–76. *Mon. Wea. Rev.*, **113,** 1970–1996.

——, and K.-M. Lau, 1986: The structure and propagation of intraseasonal oscillations appearing in a GFDL GCM. *J. Atmos. Sci.*, **43,** 2023–2047.

Livezey, R. E., and W. Y. Chen, 1983: Statistical/field significance and its determination by Monte Carlo techniques. *Mon. Wea. Rev.*, **111,** 46–59.

Lorenc, A. C., 1984: The evolution of planetary scale 200 mb divergent flow during the FGGE year. *Quart. J. Roy. Meteor. Soc.*, **110,** 427–441.

Madden, R. A., 1986: Seasonal variations of the 40–50 day oscillation in the tropics. *J. Atmos. Sci.*, **43,** 3138–3158.

——, and P. R. Julian, 1971: Detection of a 40–50 day oscillation in the zonal wind in the tropical Pacific. *J. Atmos. Sci.*, **28,** 702–708.

——, and ——, 1972: Description of global-scale circulation cells in the tropics with a 40–50 day period. *J. Atmos. Sci.*, **29,** 1109–1123.

Murakami, T., and T. Nakazawa, 1985: Tropical 45-day oscillations during the 1979 Northern Hemisphere summer. *J. Atmos. Sci.*, **42,** 1107–1122.

——, L.-X. Chen, A. Xie and M. Shrestha, 1986: Eastward propagation of 30–60 day perturbations as revealed from outgoing longwave radiation data. *J. Atmos. Sci.*, **43,** 961–971.

Mysak, L. A., and G. J. Mertz, 1984: A 40–60 day oscillation in the source region of the Somali Current during 1976. *J. Geophys. Res.*, **89,** 711–715.

Parker, D. E., 1973: Equatorial Kelvin waves at 100 millibars. *Quart. J. Roy. Meteor. Soc.*, **99,** 116–129.

Rosen, R. D., and D. A. Salstein, 1980: A comparison between circulation statistics computed from conventional data and NMC Hough Analyses. *Mon. Wea. Rev.*, **108,** 1226–1247.

Simmons, A. J., J. M. Wallace and G. W. Branstator, 1983: Barotropic wave propagation and instability, and atmospheric teleconnection patterns. *J. Atmos. Sci.*, **40,** 1363–1392.

Webster, P. J., 1972: Response of the tropical atmosphere to local, steady forcing. *Mon. Wea. Rev.*, **100,** 518–541.

Weickmann, K. M., 1983: Intraseasonal circulation and outgoing longwave radiation modes during Northern Hemisphere winter. *Mon. Wea. Rev.*, **111,** 1838–1858.

——, G. R. Lussky and J. E. Kutzbach, 1985: Intraseasonal (30–60 day) fluctuations of outgoing longwave radiation and 250 mb streamfunction during northern winter. *Mon. Wea. Rev.*, **113,** 941–961.

Yasunari, T., 1980: A quasi-stationary appearance of 30–40 day period in the cloudiness fluctuations during the summer monsoon over India. *J. Meteor. Soc. Japan,* **58,** 225–229.

——, 1981: Structure of an Indian summer monsoon system with a period around 40 days. *J. Meteor. Soc. Japan,* **59,** 336–354.